LETTERS

nature cell biology

An interaction between Scribble and the NADPH oxidase complex controls M1 macrophage polarization and function

Weiyue Zheng[1], Masataka Umitsu[1,4,5], Ishaan Jagan[1,2,5], Charles W. Tran[1,3], Noboru Ishiyama[1], Michael BeGora[1], Kiyomi Araki[1], Pamela S. Ohashi[1,3], Mitsuhiko Ikura[1] and Senthil K. Muthuswamy[1,2,6]

The polarity protein Scribble (SCRIB) regulates apical–basal polarity, directional migration and tumour suppression in *Drosophila* and mammals[1–6]. Here we report that SCRIB is an important regulator of myeloid cell functions including bacterial infection and inflammation. SCRIB interacts directly with the NADPH oxidase (NOX) complex in a PSD95/Dlg/ZO-1 (PDZ)-domain-dependent manner and is required for NOX-induced reactive oxygen species (ROS) generation in culture and *in vivo*. On bacterial infection, SCRIB localized to phagosomes in a leucine-rich repeat-dependent manner and promoted ROS production within phagosomes to kill bacteria. Unexpectedly, SCRIB loss promoted M1 macrophage polarization and inflammation. Thus, SCRIB uncouples ROS-dependent bacterial killing activity from M1 polarization and inflammatory functions of macrophages. Modulating the SCRIB–NOX pathway can therefore identify ways to manage infection and inflammation with implications for chronic inflammatory diseases, sepsis and cancer.

Downregulation of SCRIB expression in a macrophage cell line, RAW 264.7 (Fig. 1a), significantly impaired phorbol 12-myristate 13-acetate (PMA)-induced generation of ROS (Fig. 1b). In addition, we used primary macrophages from an inducible SCRIB knockdown mouse model where SCRIB short hairpin RNA (shRNA) expression was controlled by a tetracycline-response element (TRE) at the COLA1 locus (SCRIB ishRNA)[7] (Supplementary Fig. 1a). Reverse tetracycline transactivator (rtTA) expression from a ROSA26 promoter facilitated doxycycline (Dox)-inducible expression of SCRIB ishRNA and GFP in all cells, including isolated bone-marrow-derived macrophages (BMMs) (Fig. 1c). Inducible loss of SCRIB did not affect BMM differentiation as monitored by expression of CD11b/F4/80 and cell morphology (Fig. 1d and Supplementary Fig. 1b). Both PMA and lipopolysaccharide (LPS) induced ROS in wild-type cells and in SCRIB ishRNA cells in the absence of Dox stimulation (Fig. 1e). Dox-induced knockdown of SCRIB significantly impaired PMA- or LPS-induced ROS (Fig. 1e). In addition, PMA-induced ROS was significantly low in primary neutrophils (Supplementary Figs 1c,d) from Dox-treated mice (Fig. 1f), demonstrating a role for SCRIB during ROS generation in primary myeloid cells.

Apart from myeloid cells, in mouse embryo fibroblasts (MEFs) derived from SCRIB ishRNA mice (Fig. 1g) platelet-derived growth factor (PDGF)-induced generation of ROS (Fig. 1h) and tyrosine phosphorylation of the PDGF receptor were impaired (Supplementary Fig. 1e), demonstrating a role for SCRIB in regulating ROS generation in multiple contexts. The decrease in PDGFR tyrosine phosphorylation is consistent with the well-established role for ROS in inactivating tyrosine phosphatase activity and promoting tyrosine phosphorylation[8].

To determine the *in vivo* significance, SCRIB ishRNA mice were injected with LPS intraperitoneally and ROS was monitored in real time using L-012, a luminol-based chemiluminescence probe used for detecting NADPH oxidase-derived superoxide[9]. LPS challenge induced a dramatic and sustained increase in ROS levels in −Dox, but not in +Dox mice *in vivo* (Fig. 1i,j). The lack of LPS-induced ROS *in vivo* was not due to defective immune biology because cells from the thymus, spleen and bone marrow of wild-type (WT) (+Dox and −Dox) and SCRIB ishRNA (+Dox and −Dox) mice showed comparable expression of differentiation markers on dendritic, neutrophil, monocyte or B and T cells (Supplementary Figs 1f–k).

Macrophages generate ROS (superoxide (O_2^-)) using the NOX complex[10]. LPS, PMA and PDGF induce ROS by activating the NOX protein complex[11,12]. NOX-mediated generation of ROS requires

[1]Princess Margaret Cancer Center and Department of Medical Biophysics, University of Toronto, Toronto M5G 2M9, Canada. [2]Cancer Research Institute, Beth Israel Deaconess Medical Centre, Harvard Medical School, Boston, Massachusetts 02115, USA. [3]Department of Immunology, University of Toronto, Toronto M5S 1A8, Canada. [4]Present address: Institute for Protein Research, Osaka University, Osaka 565-0871, Japan. [5]These authors contributed equally to this work. [6]Correspondence should be addressed to S.K.M. (e-mail: smuthusw@bidmc.harvard.edu)

Received 24 October 2015; accepted 26 August 2016; published online 3 October 2016; DOI: 10.1038/ncb3413

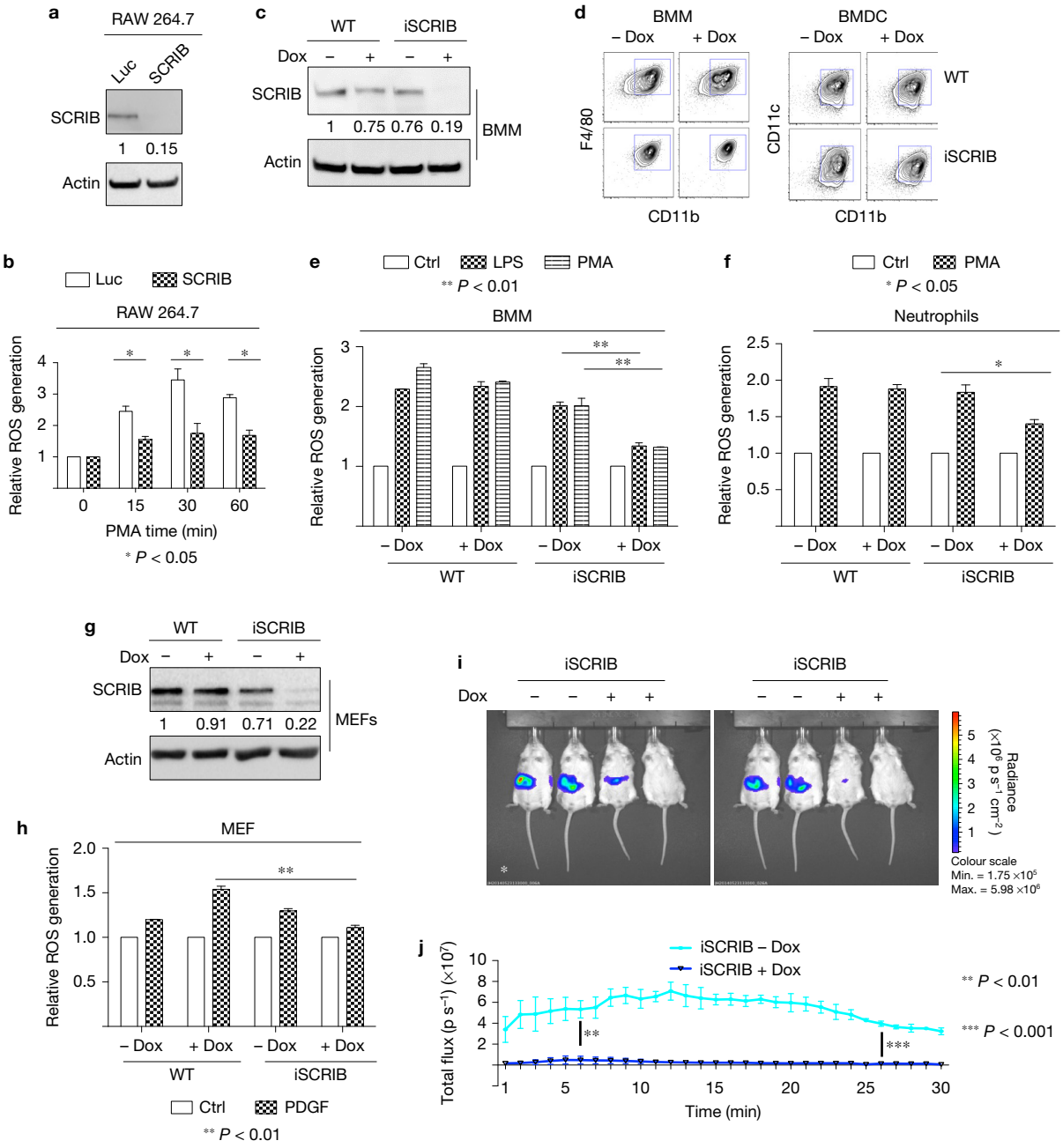

Figure 1 SCRIB is required for the generation of ROS. (**a**) Immunoblot analysis of RAW 264.7 stable cell lines expressing control Luc shRNA (Luc) or SCRIB shRNA (SCRIB). The fold change in levels is indicated. (**b**) RAW 264.7 cells stimulated with PMA and ROS generation measured by dihydroethidium at the indicated times. $n=3$ biologically independent experiments (mean ± s.d., two-tailed, unpaired *t*-test with equal variances: $P=0.024$, 0.023, 0.026). (**c**) Immunoblot analysis of Dox (1.0 μg ml^{-1})-inducible changes in SCRIB expression in BMMs isolated from WT and SCRIB ishRNA (iSCRIB) mice. (**d**) BMMs and BMDCs were stained with surface markers and analysed by flow cytometry. Representative data are shown. (**e**) BMMs stimulated with 100 ng ml^{-1} LPS or 1.0 μM PMA; ROS signal was detected by using dihydroethidium. $n=3$ biologically independent experiments (mean ± s.d., two-tailed, unpaired *t*-test with equal variances: $P=0.001$ for LPS-induced ROS and $P=0.005$ for PMA-induced ROS). (**f**) Purified primary neutrophils from WT + Dox or – Dox, and iSCRIB + Dox or – Dox mice were stimulated with PMA for 30 min and ROS generation measured by dihydroethidium at the indicated times. $n=3$ biologically independent experiments (mean ± s.d., two-tailed, unpaired *t*-test with equal variances: $P=0.022$). (**g**) Immunoblot analysis of Dox (1.0 μg ml^{-1})-inducible changes in SCRIB expression in MEFs isolated from WT and SCRIB ishRNA (iSCRIB) mice. (**h**) Relative changes in ROS levels as measured by carboxy-H2DCF-DA (DCF) in response to PDGF (50 ng ml^{-1}) for 10 min. $n=3$ biologically independent experiments (mean ± s.d., two-tailed, unpaired *t*-test with equal variances: $P=0.002$). (**i**) 8–12-week-old SCRIB ishRNA mice fed with normal or Dox food for four weeks and injected with LPS (2.0 mg kg^{-1} in PBS). Five hours post injection, L-012 (25 mg kg^{-1}) was injected into the peritoneal cavity of mice. Luminescence signal intensity was measured every minute for 30 min immediately after L-012 injection. Images shown represent an early time point (6 min; left panel) and a later time point (26 min; right panel). (**j**) Quantitative analysis of the luminescence signal intensity by Living Image software. $n=3$ animals (mean ± s.d., two-tailed, unpaired *t*-test with equal variances: $P=0.0058$, 0.00011). Source data for **b**,**e**,**f**,**h**,**j** are shown in Supplementary Table 3. All immunoblots were repeated at least three times with reproducible results. Representative images are shown. Unprocessed original scans of blots/gels are shown in Supplementary Fig. 6.

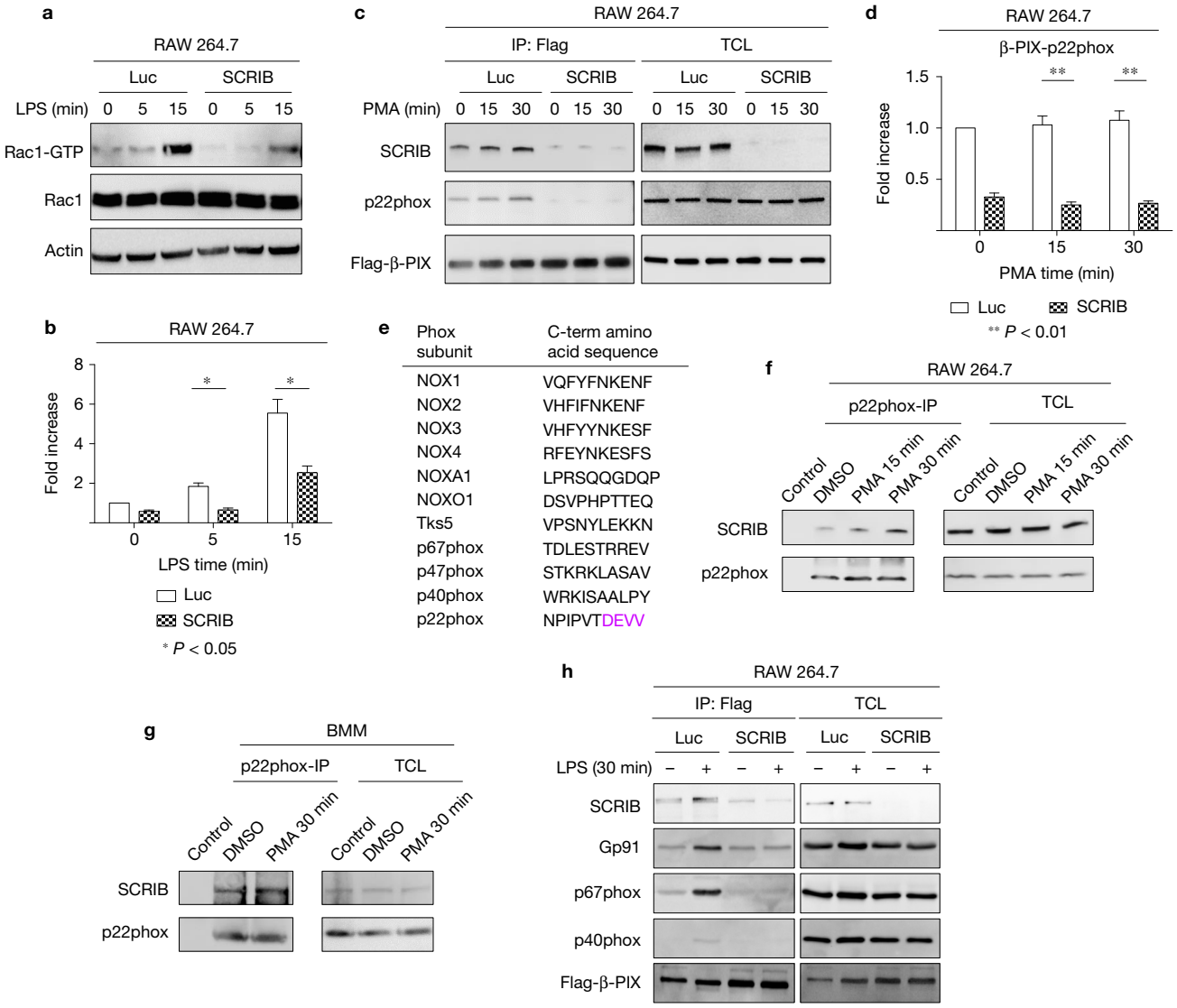

Figure 2 SCRIB is a component of the NOX complex. (**a**) Lysates from Luc shRNA (Luc) or SCRIB shRNA (SCRIB) treated with LPS (100 ng ml^{-1}) and subject to pulldown using the PAK1-p21 binding domain (PAK1-PBD) and immunoblotted for Rac1 to monitor Rac1-GTP levels (top panel). One-tenth of the input lysate was immunoblotted with Rac1 to serve as an input control. (**b**) Changes in the levels of Rac-GTP in response to LPS. $n=3$ biologically independent experiments (mean ± s.d., two-tailed, unpaired *t*-test with equal variances: $P=0.02$, 0.017). (**c**) Lysates from Luc shRNA (Luc) or SCRIB shRNA (SCRIB) RAW 264.7 cells expressing Flag-β-PIX were stimulated with PMA for the indicated times and subject to anti-Flag immunoprecipitation followed by anti-p22phox or anti-SCRIB immunoblotting. TCL, total cell lysate. (**d**) Quantitation of β-PIX levels in p22phox immunoprecipitates. $n=3$ biologically independent experiments (mean ± s.d., two-tailed, unpaired *t*-test with equal variances: $P = 0.001$, 0.001). p22phox immunoprecipitation was followed by anti-SCRIB immunoblots using lysates obtained from the parental RAW 264.7 cell line. (**e**) Amino acid sequence alignment of the carboxy tail of members of the NOX complex. (**f**,**g**) p22phox immunoprecipitates from parental RAW 264.7 cells (**f**), or BMMs (**g**) were immunoblotted for anti-SCRIB. DMSO, dimethyl sulfoxide. (**h**) Lysates from Luc shRNA (Luc) or SCRIB shRNA (SCRIB) RAW 264.7 cells expressing Flag-β-PIX were stimulated with LPS and subject to anti-Flag immunoprecipitation followed by anti-Gp91, p67phox, p40phox or anti-SCRIB immunoblotting. Source data for **b**,**d** are shown in Supplementary Table 3. All immunoblots were repeated at least three times with reproducible results. Representative images are shown. Unprocessed original scans of blots/gels are shown in Supplementary Fig. 6.

activation of Rac GTPases facilitated by the GTP exchange factor β-PIX[13]. Since β-PIX binds directly with SCRIB, LPS-induced Rac activation was analysed in SCRIB shRNA cells. Interestingly, LPS-induced Rac.GTP levels were twofold lower in SCRIB shRNA cells compared with Luc shRNA cells (Fig. 2a,b).

We tested whether SCRIB functions as a scaffold to recruit β-PIX to the NOX complex. β-PIX co-immunoprecipitated both p22phox (a component of the NOX complex) and SCRIB in Flag-tagged β-PIX-expressing control cells, but not in RAW 264.7 SCRIB shRNA cells. The interaction was observed both before and after PMA stimulation, with a modest increase in association post PMA stimulation (Fig. 2c,d and Supplementary Fig. 2a).

SCRIB is a PSD95/Dlg/ZO-1 (PDZ)-domain-containing protein and PDZ domains frequently use carboxy-terminal residues to interact with its partners. Analysis of the carboxy-terminal 10 amino acids of all members of the NOX complex showed that only the C-terminal

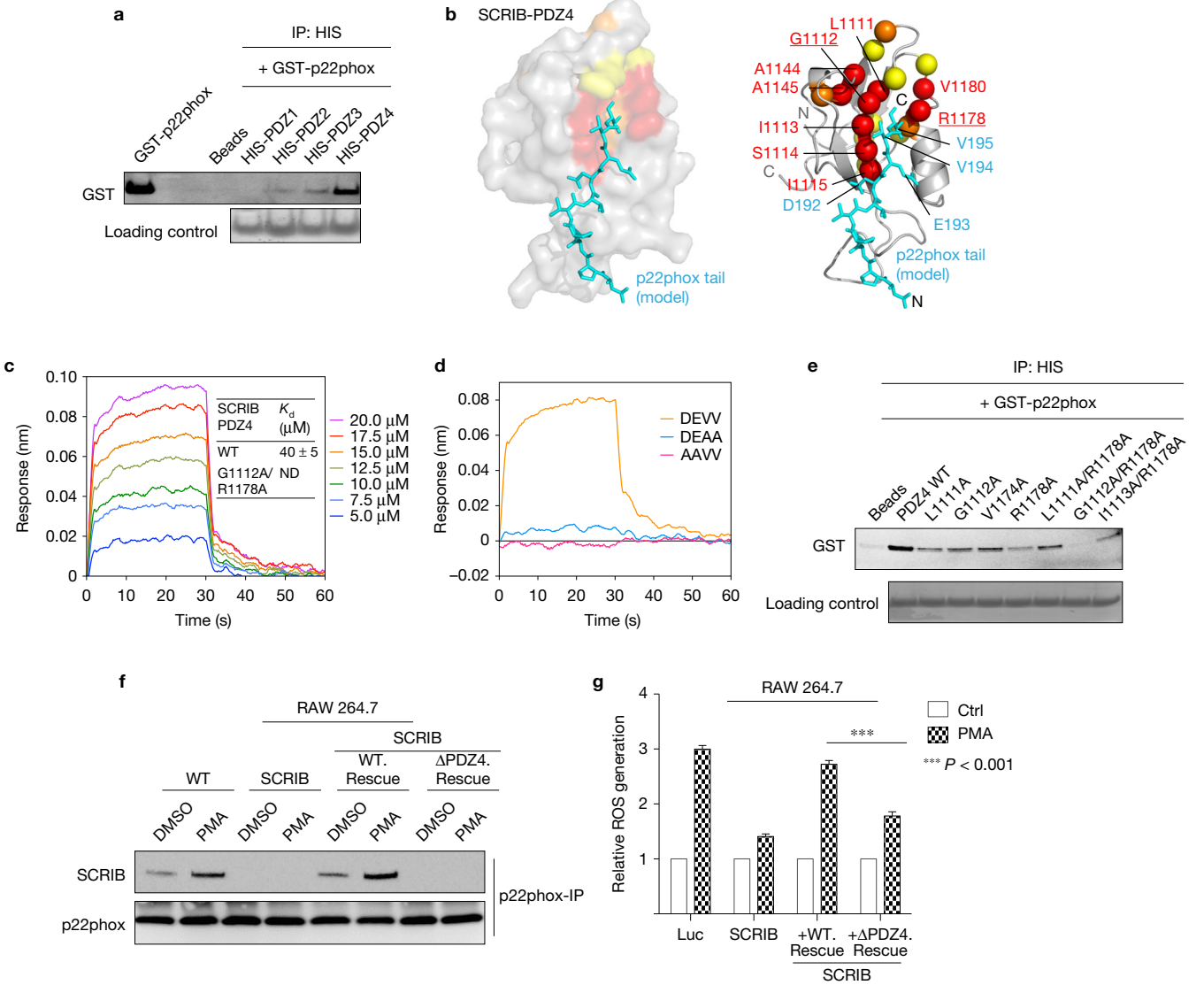

Figure 3 SCRIB interacts directly with p22phox and promotes PMA-induced generation of ROS. (**a**) HIS-PDZ domains incubated with the GST-p22 carboxyl tail and pulldowns were immunoblotted with anti-GST antibodies. Coomassie blue staining of input HIS-tagged protein was used as a loading control and HIS beads incubated with GST-p22tail were used as a negative control. (**b**) The SCRIB-PDZ4-p22phox tail-docking model was generated using the hSCRIB-PDZ4 domain (PDB ID 1UJU) as a template for SCRIB-PDZ4 (P1096-E1193) and the Erbin PDZ domain-ErbB2 (PDB ID 1MFG) for the p22phox chain model that was built using Coot[34] and Pymol (http://www.pymol.org) software. SCRIB-PDZ4 residues affected by the addition of the p22phox tail peptide are mapped and indicated as spheres on the modelled structure of the SCRIB-PDZ4 domain (red: >0.2 normalized chemical shift change, orange: 0.2–0.14 and yellow: 0.1–0.14, respectively). The modelled p22phox tail is shown as a stick model, coloured as cyan. The four C-terminal residues of p22phox (192-DEVV-195) are indicated. (**c**) BLI response curves representing the association (0–30 s) and dissociation (30–60 s) of WT SCRIB-PDZ4 in the concentration range of 5–20 μM with the biotinylated p22phoxC10 peptide immobilized on the streptavidin-coated sensors. Binding curve analysis using a 1:1 binding model revealed that WT SCRIB-PDZ4 binds to p22phoxC10 with a dissociation constant (K_d) of 40 ± 5 μM. ND, no detectable binding. (**d**) Comparison of response curves of SCRIB-PDZ4 association with the WT (DEVV) and two mutant (DEAA and AAVV) variants of p22phoxC10. The response curve was obtained with 20 μM SCRIB-PDZ4 proteins. (**e**) SCRIB-PDZ4 domain wild type (PDZ4 WT) or with mutations (indicated as amino acid number and one letter abbreviation) that were predicted to affect interaction with p22phox peptide were expressed as HIS-tagged fusions and incubated with the GST-p22 carboxyl tail. Coomassie blue staining of input HIS-tagged PDZ domains was used as a loading control. (**f**) Anti-p22phox immunoprecipitates from lysates simulated with PMA for 30 min were immunoblotted with anti-SCRIB antibodies. (**g**) Relative ROS generation in RAW 264.7 cells either lacking SCRIB expression (SCRIB) or rescued with WT SCRIB cDNA (WT.Rescue), or SCRIB-PDZ4 domain (G1112A/R1178A) (ΔPDZ4.Rescue). $n = 3$ biologically independent experiments (mean ± s.d., two-tailed, unpaired t-test with equal variances: $P = 0.00079$). Source data for **g** are shown in Supplementary Table 3. All immunoblots were repeated at least three times with reproducible results. Representative images are shown. Unprocessed original scans of blots/gels are shown in Supplementary Fig. 6.

sequence of p22phox (192-DEVV-195) conforms to a class III PDZ-binding motif (X(unspecified)-D/E-X-Ψ(hydrophobic))[14] (Fig. 2e). Amino-terminal Flag-tagged WT p22phox, but not the p22phox lacking the C-terminal 10 amino acids (p22Δ), interacted with T7 epitope-tagged SCRIB (Supplementary Fig. 2b). p22phox is a common subunit present in all of the NOX complexes (NOX1–4) (Supplementary

Fig. 2c); accordingly, SCRIB co-immunoprecipitated with NOXO1 (a component of NOX1 and 3) and Tks5 (a component of NOX4) (Supplementary Figs 2d,e), identifying SCRIB as a member of all NOX complexes. Both the NOX1 and NOX3 complexes require Rac.GTP for their activity, supporting a role for SCRIB in these complexes[15].

Endogenous p22phox from both RAW 264.7 (Fig. 2f) and primary BMMs (Fig. 2g) was able to co-immunoprecipitate SCRIB. Conversely, endogenous SCRIB co-immunoprecipitated p22phox (Supplementary Fig. 2f). In contrast to SCRIB–p22phox association (Supplementary Figs 2g,h), interaction with other components of the NOX complex, gp91phox, p67phox and p40phox, was induced on LPS stimulation in a SCRIB-dependent manner (Fig. 2h). This is consistent with previous observations that LPS stimulation induces assembly of an active NOX complex[16].

To determine whether SCRIB and p22phox interact directly with each other, we used bacterially produced 6xHis-tag fusions of each of the four PDZ domains (SCRIB-PDZ1, SCRIB-PDZ2, SCRIB-PDZ3 and SCRIB-PDZ4) (Supplementary Fig. 3a) and GST-tag-fused p22phox C-terminal tail (186-NPIPVTDEVV-195) (p22tail). Purified SCRIB-PDZ4, but not the other PDZ domains, bound directly to purified p22tail (Fig. 3a). Next we performed a nuclear magnetic resonance (NMR) spectroscopy experiment on ^{15}N-labelled SCRIB-PDZ4 with unlabelled p22tail peptide (residues 186–195) to identify the binding interface (Supplementary Fig. 3b). By increasing the concentration of the peptide, we observed nine peaks displaying marked peak shifts (>0.2 normalized chemical shift change) in the ^{1}H-^{15}N heteronuclear single-quantum coherence spectra (Supplementary Fig. 3c). We then mapped these perturbed residues (Leu1111, Gly1112, Ile1113, Ser1114, Ile1115, Ala1144, Ala1145, Arg1178 and Val1180) onto the previously reported three-dimensional structure of unligated SCRIB-PDZ4 (PDB: 1UJU) (Supplementary Figs 3d–f). In contrast, a p22phox peptide lacking the carboxy tail (residues 131–185) displayed no change in the NMR spectra of SCRIB-PDZ4 (Supplementary Figs 3g,h). A typical PDZ domain consists of six β-strands (βA–βF) and two α-helices (αA and αB). The most affected residues Leu1111 and Gly1112 are located in the well-known target-carboxylate binding loop (1110-RLGI-1113), while other perturbed residues, Ser1114 and Ile1115, reside at the βB strand and Arg1178 is located within the αB helix. The identified p22tail binding site on SCRIB-PDZ4 coincides well with the canonical target-binding pocket found in many PDZ proteins[17]. Accordingly we generated a p22tail-docking model structure of SCRIB-PDZ4 (Fig. 3b) using the structure of the Erbin PDZ domain-ErbB2 peptide complex (PDB 1MFG[18]) as a template.

We next used bio-layer interferometry (BLI), an optical sensing technique used to measure macromolecular interactions, and determined the dissociation constant (K_d) of SCRIB-PDZ4-p22phox peptide to be $40 \pm 5\,\mu M$ (Fig. 3c). To examine the specificity of the interaction of the PDZ4-p22phox C termini, we generated two variants of the peptides, DEAA and AAVV. Compared with the wild-type peptide, DEVV, the variants had no detectable binding in the BLI assay (Fig. 3d). To generate mutants of SCRIB that do not interact with p22phox, we designed single and double alanine substitutions for residues Leu1111, Gly1112, Ile1113, Ile1174 and Arg1178 in SCRIB-PDZ4, based on the SCRIB-PDZ4-p22phox tail-docking model (Fig. 3b). GST-pulldown and NMR experiments demonstrated that the G1112A/R1178A double mutant inhibited binding of p22tail to SCRIB-PDZ4 (Fig. 3e). Consistent with this observation, the double mutant neither produced the chemical shift observed for WT PDZ4 (Supplementary Figs 3i,j) nor showed interaction in the BLI assay (Supplementary Fig. 3k). The loss in binding was not due to protein/domain folding defects, as supported by circular dichroism spectroscopy, which indicated that the secondary structures are retained in the G1112A/R1178A mutant (Supplementary Fig. 3l). We rescued SCRIB shRNA RAW 264.7 cells with RNAi-resistant SCRIB WT and PDZ4 mutant G1112A/R1178A (ΔPDZ4). Expression of SCRIB-ΔPDZ4 in SCRIB shRNA cells did not rescue p22phox-SCRIB demonstrating that PDZ4 was required for SCRIB–p22phox interaction *in vivo* (Fig. 3f). Functionally, SCRIB shRNA cells rescued with WT SCRIB, but not the cells rescued with ΔPDZ4 mutant, upregulated ROS (Fig. 3g) in response to stimulation with PMA. Thus, the PDZ4 domain of SCRIB is essential for interaction with the NOX complex and for the SCRIB-dependent production of ROS.

NOX complex-generated respiratory burst within phagosomes is required to kill invading bacteria[19]. To investigate whether loss of SCRIB affects the ability of phagocytes to clear bacterial infection, we challenged SCRIB ishRNA mice with an intraperitoneal injection of *Staphylococcus aureus* (Fig. 4a). SCRIB ishRNA−Dox mice were fourfold more effective in clearing *S. aureus* from both the peritoneal cavity and the lung compared with mice on a Dox diet (Fig. 4b,c). To rule out a role for differences in neutrophil migration, we analysed purified neutrophils (Fig. 4d) and blood preparations (Supplementary Figs 4a,b) from SCRIB ishRNA+Dox or −Dox mice in culture and show that myeloid cells from +Dox mice have a fourfold decrease in *S. aureus* killing compared with cells from SCRIB ishRNA−Dox or WT mice, demonstrating a cell-intrinsic defect. Furthermore, both RAW 264.7 control and SCRIB shRNA cells were equally competent in internalizing pHrodo dye-conjugated *S. aureus* particles demonstrating that bacterial phagocytosis was unaffected by loss of SCRIB (Fig. 4e,f).

Next, we investigated the relationship between SCRIB and phagosomes. Structured illumination microscopy of RAW 264.7 cells 1.0 h post *S. aureus* infection demonstrated co-localization of SCRIB and p22phox around *S. aureus* (Fig. 4g). Both the PDZ4 mutant and WT SCRIB, expressed in the background of SCRIB shRNA, were effective in localizing to the bacteria (Fig. 4h), demonstrating that SCRIB–p22phox interaction was not required for SCRIB to localize to phagosomes (Fig. 4i). In both SCRIB WT and PDZ4 rescue cell lines, SCRIB was localized at a comparable distance to bacteria (median distance between 1.5–2.0 μm), as monitored by conventional confocal image analysis (Fig. 4j). In addition to RAW 264.7 cells, SCRIB accumulated near bacteria containing phagosomes in a human macrophage cell line Thp1 expressing RFP-SCRIB and infected with FITC-*S. aureus* (Supplementary Figs 4c–e) demonstrating evolutionary conservation of the mechanism.

In both *Drosophila* and mammalian epithelial cells, SCRIB regulates cell polarity in a membrane localization-dependent manner[3,20,21]. A SCRIB mutant that fails to localize to the cell membrane[20,21], Pro305 to leucine (P305L), also failed to localize near bacteria (Fig. 4i), identifying a role for membrane localization in localizing SCRIB to phagosomes. Neither PDZ4 nor SCRIBP305L expression in RAW 264.7 SCRIB shRNA cells rescued PMA-induced

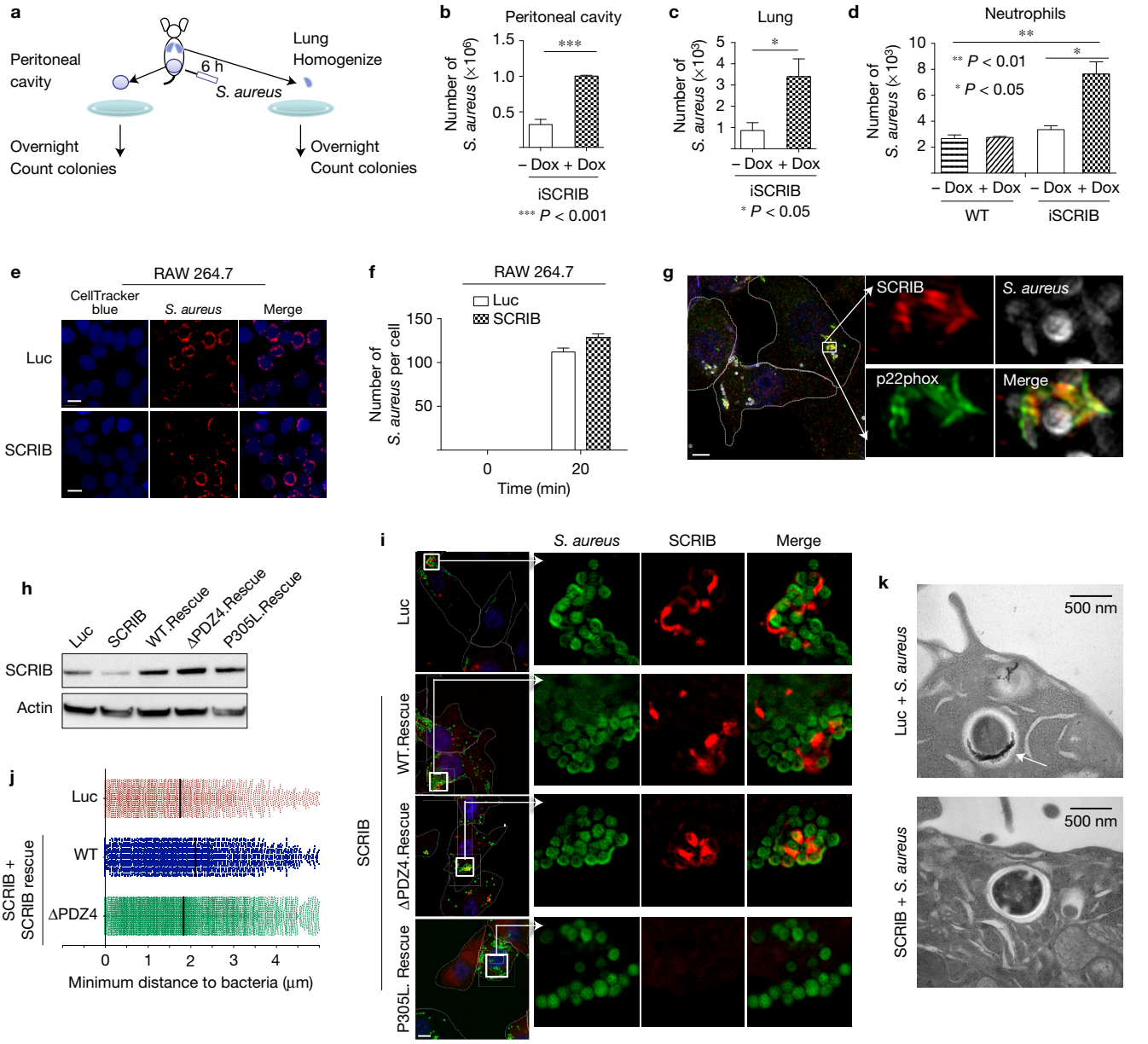

Figure 4 SCRIB is required for clearing *S. aureus* infection *in vivo* and is recruited to phagosomes. (**a**) A schematic diagram of the experimental design for mouse infection. Mice (8–12 week old, $n=3$) were infected intraperitoneally with *S. aureus* (2×10^8 colony-forming units (CFUs)). (**b**,**c**) After 6.0 h, CFUs were determined using peritoneal cavity that was lavaged (**b**), or from homogenized lung tissue (**c**). $n=3$ biologically independent animals (mean ± s.d., two-tailed, unpaired *t*-test with equal variances: $P=0.00078$ (**b**), $P=0.049$ (**c**). (**d**) Purified primary neutrophils from WT, SCRIB ishRNA (iSCRIB) + Dox or − Dox mice were incubated with *S. aureus* for 20 min. Lysostaphin was added at 20 min of incubation and aliquots were removed at 60 min for enumeration of *S. aureus* CFUs. $n=3$ biologically independent animals (mean ± s.d., two-tailed, unpaired *t*-test with equal variances: $P=0.012$). (**e**) Cells were imaged every 40 s for 2.0 h to measure *S. aureus* uptake. Representative images at 0 and 20 min are shown. Blue is CellTracker blue dye; red is pHrodo-red-conjugated *S. aureus*. The right panels show representative merge images. Scale bars, 10 μm. (**f**,**g**) Quantification of *S. aureus* per cell (**f**) and structured illumination micrographs (**g**) of RAW 264.7 cells incubated with *S. aureus* (grey) for 1 h fixed and stained for SCRIB (red) and p22phox (green); $n=3$ biologically independent experiments (mean ± s.d., two-tailed, unpaired *t*-test with equal variances). Scale bar, 5 μm. (**h**) RAW 264.7 cells expressing Luc shRNA (Luc) or SCRIB shRNA (SCRIB) or SCRIB shRNA cells expressing WT SCRIB (WT.Rescue), or mutant PDZ4 domain (G1112A/R1178A) (ΔPDZ4.Rescue), or mutant LRR domain (P305L.Rescue). (**i**) RAW 264.7 cells expressing SCRIB shRNA (SCRIB) and rescued with WT SCRIB (WT.Rescue) or p305L SCRIB (P305L. Rescue) or PDZ4 mutant (ΔPDZ4.Rescue) were incubated with *S. aureus* (green) and stained for SCRIB (red). The three right panels are enlarged views of the boxed regions in the left panels. Scale bar, 10 μm. (**j**) Quantification of the minimum distance between *S. aureus* and enriched SCRIB in SCRIB shRNA (SCRIB) and rescue (SCRIB WT, PDZ4 mutant (ΔPDZ4)) from the images. Individual SCRIB enrichment events around bacteria are plotted as red triangles for Luc shRNA (Luc), blue squares for SCRIB WT rescue and green circles for SCRIB-PDZ4 mutant rescue. The solid black bars represent the median minimum distance from bacteria to SCRIB for three replicates; $n=750$ pooled from three independent biological replicates. (**k**) Representative transmission electron micrograph of *S. aureus*-containing phagosomes 1 h post infection in Luc shRNA (Luc) and SCRIB shRNA (SCRIB) RAW 264.7 cells. Arrow points to the cerium ion precipitates. Source data for **b**–**d**,**f** are shown in Supplementary Table 3. All immunoblots were repeated at least three times with reproducible results. Representative images are shown. Unprocessed original scans of blots/gels are shown in Supplementary Fig. 6.

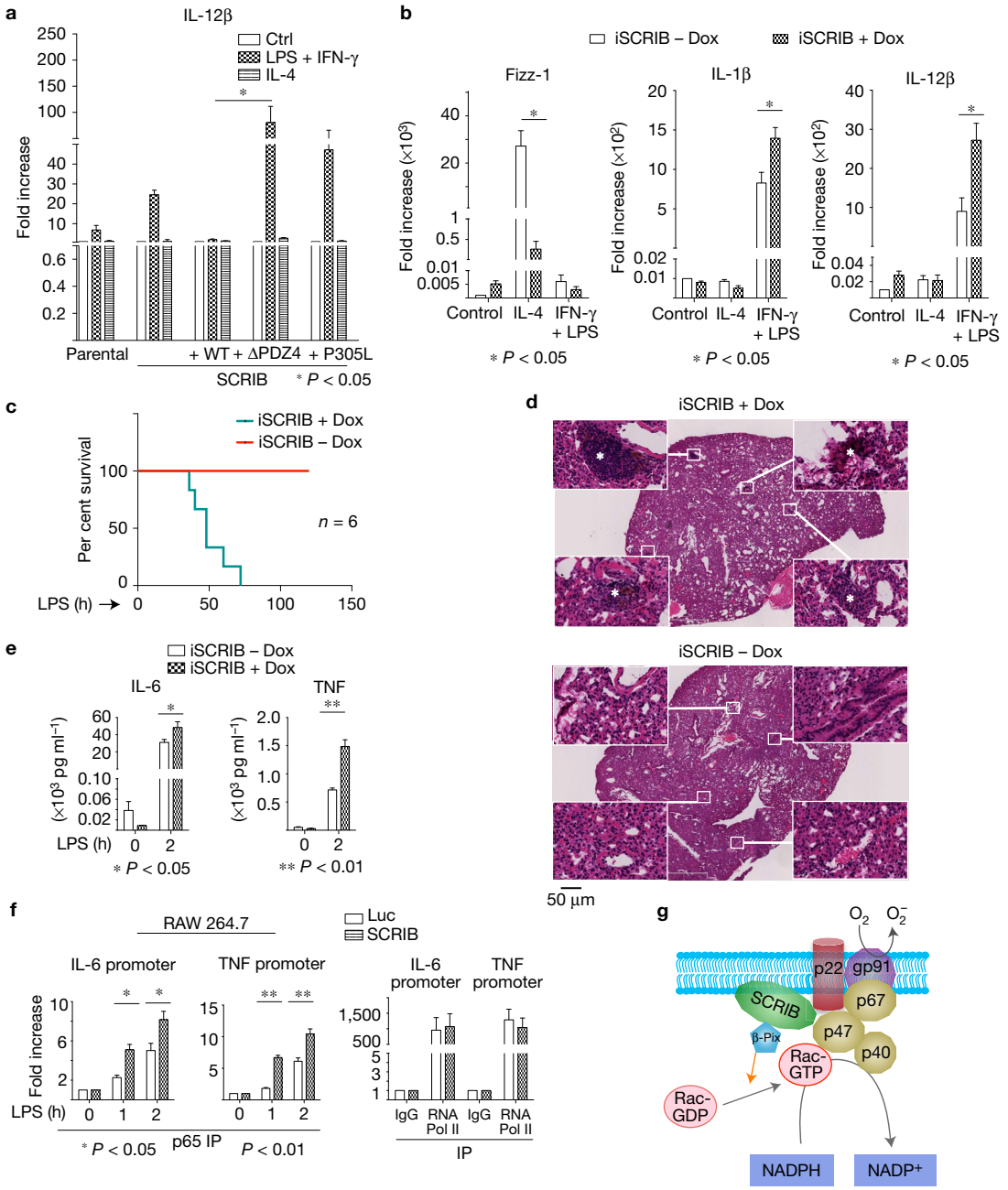

Figure 5 SCRIB regulated inflammatory response. (**a**) Quantitative PCR analysis of M1 (IL-12β) and macrophage markers in parental RAW 264.7, SCRIB shRNA (SCRIB) cells, and cells rescued with WT SCRIB or PDZ4 mutant or P305L after induction of M1 (IFN-γ + LPS) fate. $n=3$ biologically independent experiments (mean ± s.d., two-tailed, unpaired t-test with equal variances: $P=0.02$). (**b**) Quantitative PCR analysis of M1 (IL-1β, IL-12β) and M2 (Fizz-1) macrophage markers in BMMs derived from SCRIB ishRNA (iSCRIB) − Dox and SCRIB ishRNA (iSCRIB) + Dox after induction of M1 (IFN-γ + LPS) or M2 (IL-4) fates. $n=3$ biologically independent experiments (mean ± s.d., two-tailed, unpaired t-test with equal variances: $P=0.014$, 0.041, 0.03). (**c**) The ishSCRIB mice (8–12 weeks old) injected intraperitoneally with either LPS (2 mg kg^{-1} in PBS) or PBS alone (control). $n=6$ animals. Kaplan–Meier curve showing survival of mice over 120 h (5 days). (**d**) Representative H&E-stained image of lung tissues 24 h post LPS injection. Asterisks mark areas with immune cell infiltrates. (**e**) The amount of IL-6 and TNF in the blood of mice used in **c** was quantitated using enzyme-linked immunosorbent assay. $n=3$ biologically independent animals (mean ± s.d., two-tailed, unpaired t-test with equal variances: $P=0.044$, 0.0035). (**f**) Chromatin immunoprecipitation analysis using anti-p65 or anti-Pol II antibodies on IL-6 or TNF promoters. $n=3$ biologically independent experiments (mean ± s.d., two-tailed, unpaired t-test with equal variances: $P=0.042$, 0.048 (IL-6); $P=0.0012$, 0.0031 (TNF)). (**g**) Cartoon model of SCRIB interaction with the NOX complex generating ROS. Source data for **a**–**c**,**e**,**f** are shown in Supplementary Table 3.

generation of ROS (Fig. 3f and Supplementary Fig. 4f), suggesting that both interaction with p22phox and localization to the phagosome were required for ROS generation.

Generation of ROS within the phagosome is required for the ability of macrophages to kill bacteria[22]. RAW 264.7 Luc shRNA and SCRIB shRNA cells were infected with *S. aureus* and incubated

with cerium chloride, which reacts with ROS in phagosomes to form an electron-dense precipitate visible by transmission electron microscopy[23]. Electron-dense precipitates of cerium ions were found around the *S. aureus*-containing phagosomes in shLuc cells, but not SCRIB shRNA cells (Fig. 4k), identifying an unexpected role for SCRIB as a regulator of ROS generation within phagocytic structures.

We next investigated whether SCRIB regulates macrophage polarization because M1 macrophages are key regulators of host defence to pathogen infection and inflammation[24]. RAW 264.7 and primary, bone marrow-derived, cells were stimulated with a combination of interferon gamma and LPS to induce M1 or IL-4 to induce M2 macrophage polarization. Surprisingly, cells lacking SCRIB (+Dox) showed a significant increase in the tendency to polarize towards the M1 lineage, as monitored by expression of IL-1β and Il-12β messenger RNA, but a decrease in the tendency to polarize towards the M2 lineage, as monitored by Fizz-1 mRNA expression (Fig. 5a,b). This phenotype was rescued by re-expression of SCRIB WT, but not by expression of PDZ4 or P305L mutants (Fig. 5a), demonstrating the need for p22phox interaction and membrane localization. Thus, the impaired bacterial killing in mice lacking SCRIB is not due to a defect in M1 polarization.

The enhanced M1 polarization associated with SCRIB loss, but the defect in the ability to kill bacteria, raised the possibility that these M1 macrophages may not be functional. To investigate this possibility, LPS (2 mg kg^{-1}) was administered intraperitoneally into SCRIB ishRNA+Dox and SCRIB ishRNA−Dox mice. Surprisingly, LPS injection induced a lethal response within 72 h in 100% mice lacking SCRIB (+Dox). None of the mice with normal levels of SCRIB (−Dox) had an adverse response for six days following LPS challenge (the longest time point followed) (Fig. 5c). Thus, the M1 macrophages lacking SCRIB were highly competent to mount a lethal inflammatory response on LPS stimulation. To better understand the inflammatory response, we isolated lung tissue 24 h post LPS injection from SCRIB ishRNA+Dox and −Dox mice. Immune cell infiltration was increased in SCRIB ishRNA+Dox compared with SCRIB ishRNA−Dox (Fig. 5d) mouse lung as monitored by haematoxylin and eosin (H&E) staining.

To determine whether the hyper-inflammatory response relates to enhanced cytokine production, we cultured BMMs from SCRIB ishRNA mice, stimulated them with LPS for 2.0 h and assayed for mRNA expression of inflammatory cytokines using quantitative PCR arrays. Pro-inflammatory cytokines were upregulated in SCRIB ishRNA+Dox compared with SCRIB ishRNA−Dox cells (2–10-fold) on LPS challenge (Supplementary Fig. 5a). Consistent with the increase in transcript levels, protein levels of the major inflammatory cytokines, IL-6 and TNF (also known as TNFα), were significantly higher in SCRIB ishRNA+Dox mice compared with −Dox conditions (Fig. 5e). Inflammatory cytokines are primarily induced by the NF-κB transcription complex[25]. However, neither the phosphorylation of IkB-alpha nor nuclear localization of p65 was altered by SCRIB loss (Supplementary Fig. 5b,c). ROS can oxidize Cys62 of the p50 subunit of NF-κB ROS and interfere with its DNA-binding ability[26]. Thus, the low levels of LPS-induced ROS in SCRIB knockdown cells can paradoxically increase the DNA-binding capacity of NF-κB to DNA and promote expression of inflammatory cytokines. Consistent with this possibility, the p65 subunit of the NF-κB complex was bound at significantly higher levels on both the IL-6 and TNF promoter in cells lacking SCRIB (Fig. 5f) as determined by chromatin immunoprecipitation (ChIP). However, polymerase II occupancy on these promoters was not affected by loss of SCRIB. In addition to macrophages, dendritic cells are also sensitive to differences in ROS levels[27]. Dendritic cells with low levels of ROS show a heightened response to LPS challenge compared with those with high levels of ROS[28]. Bone-marrow-derived dendritic cells (BMDCs) showed an elevated expression of canonical activation markers, such as CD80, CD86 and MHCII, in the absence of SCRIB expression (+Dox) and with LPS stimulation (Supplementary Figs 5d,e). Thus, loss of SCRIB results in increased DC sensitivity to LPS stimulation, which potentially exacerbates the hyper-inflammatory phenotype and lethal response observed with LPS challenge of ishSCRIB+Dox mice.

In addition to its role in the clearance of bacterial infections, NADPH oxidase is also an important regulator of inflammation. Individuals with chronic granulomatous disease, caused by mutations in members of the NOX complex, show hyper-inflammatory symptoms such as development of granuloma, Crohn's-like disease and pulmonary fibrosis[29–31]. p47phox knockout mice, in addition to having a defect in clearing bacterial infection due to decreased generation of ROS, show a hyper-inflammatory response on LPS challenge[32]. Our observations are thus consistent with the phenotypes observed in patients with a defective NOX complex and those reported for mouse models with mutations in the NOX complex, providing genetic support to our conclusion that SCRIB is a member of the NOX complex (Fig. 5g). In addition, we report an unexpected finding that SCRIB is a regulator of M1/M2 polarization. Thus, we define a function for SCRIB in cells of the myeloid lineage. Apart from myeloid cells, the NOX complex plays an important role in the central nervous system including microglia function, astrocyte survival, neuronal polarization, axonal growth and neurodegenerative disease[15,33]. Thus, a better understanding of the SCRIB–NOX pathway can provide insights into neurological diseases, managing bacterial infection, modulating inflammation and tumour cell killing with implications for chronic inflammatory diseases, sepsis and cancer. □

METHODS

Methods, including statements of data availability and any associated accession codes and references, are available in the online version of this paper.

Note: Supplementary Information is available in the online version of the paper

ACKNOWLEDGEMENTS

We would like to thank S. Courtneidge (Oregon Health and Science University, USA) for Tks5, NOXA1 and NoxO1 cDNA, I. Harris for assistance with ROS assays, G. M. C. Gasmi-Seabrook for assistance with NMR experiments, P. B. Stathopulos for assistance in structural modelling and its analysis, and members of the Muthuswamy laboratory for critical discussions. This work was supported by CA098830, BC075024, Era of Hope Scholar award from DOD Breast Cancer Research Program; Rita Allen Foundation, Lee K Margaret Lau Chair for breast cancer research and Campbell Family Institute for Breast cancer research to S.K.M. M.U. received fellowships from The Uehara Memorial Foundation, The Naito Foundation, and the Terry Fox Foundation EIRR21 at CIHR, and a JSPS postdoctoral fellowship for research abroad. This was also funded in part by the Ontario Ministry of Health and Long Term Care. The views expressed do not necessarily reflect those of the OMOHLTC.

AUTHOR CONTRIBUTIONS

W.Z. was responsible for the study, performed the majority of the experiments, analysed data and assisted with writing of the manuscript. M.U., N.I. and M.I. planned, performed, analysed and wrote the NMR studies. I.J. performed image acquisition and analysis and worked together with W.Z. and assisted with writing the manuscript. K.A. and M.B. were involved in maintaining the mouse colony. C.W.T. and P.S.O. planned, performed and analysed dendritic cell studies. S.K.M. conceptualized and executed the study and wrote the manuscript.

COMPETING FINANCIAL INTERESTS

The authors declare no competing financial interests.

Published online at http://dx.doi.org/10.1038/ncb3413
Reprints and permissions information is available online at www.nature.com/reprints

1. Bilder, D., Li, M. & Perrimon, N. Cooperative regulation of cell polarity and growth by *Drosophila* tumor suppressors. *Science* **289,** 113–116 (2000).
2. Cordenonsi, M. *et al.* The Hippo transducer TAZ confers cancer stem cell-related traits on breast cancer cells. *Cell* **147,** 759–772 (2011).
3. Feigin, M. E. *et al.* Mislocalization of the cell polarity protein scribble promotes mammary tumorigenesis and is associated with basal breast cancer. *Cancer Res.* **74,** 3180–3194 (2014).
4. Zhan, L. *et al.* Deregulation of scribble promotes mammary tumorigenesis and reveals a role for cell polarity in carcinoma. *Cell* **135,** 865–878 (2008).
5. Pearson, H. B. *et al.* SCRIB expression is deregulated in human prostate cancer, and its deficiency in mice promotes prostate neoplasia. *J. Clin. Invest.* **121,** 4257–4267 (2011).
6. Elsum, I. A. *et al.* Scrib heterozygosity predisposes to lung cancer and cooperates with KRas hyperactivation to accelerate lung cancer progression *in vivo*. *Oncogene* **33,** 5523–5533 (2014).
7. Baker, L. *et al.* SCRIBBLE is required for pregnancy-induced alveologenesis in the adult mammary gland. *J. Cell Sci.* **129,** 2307–2315 (2016).
8. Meng, T. C., Fukada, T. & Tonks, N. K. Reversible oxidation and inactivation of protein tyrosine phosphatases *in vivo*. *Mol. Cell* **9,** 387–399 (2002).
9. Nishinaka, Y. *et al.* A new sensitive chemiluminescence probe, L-012, for measuring the production of superoxide anion by cells. *Biochem. Biophys. Res. Commun.* **193,** 554–559 (1993).
10. Babior, B. M., Kipnes, R. S. & Curnutte, J. T. Biological defense mechanisms. The production by leukocytes of superoxide, a potential bactericidal agent. *J. Clin. Invest.* **52,** 741–744 (1973).
11. Park, H. S. *et al.* Cutting edge: direct interaction of TLR4 with NAD(P)H oxidase 4 isozyme is essential for lipopolysaccharide-induced production of reactive oxygen species and activation of NF-κB. *J. Immunol.* **173,** 3589–3593 (2004).
12. Segal, A. W. & Abo, A. The biochemical basis of the NADPH oxidase of phagocytes. *Trends Biochem. Sci.* **18,** 43–47 (1993).
13. Knaus, U. G., Heyworth, P. G., Evans, T., Curnutte, J. T. & Bokoch, G. M. Regulation of phagocyte oxygen radical production by the GTP-binding protein Rac 2. *Science* **254,** 1512–1515 (1991).
14. Nourry, C., Grant, S. G. & Borg, J. P. PDZ domain proteins: plug and play!. *Sci. STKE* **2003,** re7 (2003).
15. Bedard, K. & Krause, K. H. The NOX family of ROS-generating NADPH oxidases: physiology and pathophysiology. *Physiol. Rev.* **87,** 245–313 (2007).
16. Groemping, Y., Lapouge, K., Smerdon, S. J. & Rittinger, K. Molecular basis of phosphorylation-induced activation of the NADPH oxidase. *Cell* **113,** 343–355 (2003).
17. Lee, H. J. & Zheng, J. J. PDZ domains and their binding partners: structure, specificity, and modification. *Cell Commun. Signal.* **8,** 8 (2010).
18. Birrane, G., Chung, J. & Ladias, J. A. Novel mode of ligand recognition by the Erbin PDZ domain. *J. Biol. Chem.* **278,** 1399–1402 (2003).
19. Segal, A. W. How neutrophils kill microbes. *Annu. Rev. Immunol.* **23,** 197–223 (2005).
20. Bilder, D. & Perrimon, N. Localization of apical epithelial determinants by the basolateral PDZ protein Scribble. *Nature* **403,** 676–680 (2000).
21. Audebert, S. *et al.* Mammalian Scribble forms a tight complex with the βPIX exchange factor. *Curr. Biol.* **14,** 987–995 (2004).
22. Lam, G. Y. *et al.* Listeriolysin O suppresses phospholipase C-mediated activation of the microbicidal NADPH oxidase to promote *Listeria monocytogenes* infection. *Cell Host Microbe* **10,** 627–634 (2011).
23. Briggs, R. T., Drath, D. B., Karnovsky, M. L. & Karnovsky, M. J. Localization of NADH oxidase on the surface of human polymorphonuclear leukocytes by a new cytochemical method. *J. Cell Biol.* **67,** 566–586 (1975).
24. Benoit, M., Desnues, B. & Mege, J. L. Macrophage polarization in bacterial infections. *J. Immunol.* **181,** 3733–3739 (2008).
25. Lawrence, T. The nuclear factor NF-κB pathway in inflammation. *Cold Spring Harb. Perspect. Biol.* **1,** a001651 (2009).
26. Matthews, J. R., Wakasugi, N., Virelizier, J. L., Yodoi, J. & Hay, R. T. Thioredoxin regulates the DNA binding activity of NF-κB by reduction of a disulphide bond involving cysteine 62. *Nucleic Acids Res.* **20,** 3821–3830 (1992).
27. Sattler, M. *et al.* Hematopoietic growth factors signal through the formation of reactive oxygen species. *Blood* **93,** 2928–2935 (1999).
28. Sheng, K. C., Pietersz, G. A., Tang, C. K., Ramsland, P. A. & Apostolopoulos, V. Reactive oxygen species level defines two functionally distinctive stages of inflammatory dendritic cell development from mouse bone marrow. *J. Immunol.* **184,** 2863–2872 (2010).
29. Dinauer, M. C. & Orkin, S. H. Chronic granulomatous disease. *Annu. Rev. Med.* **43,** 117–124 (1992).
30. Rieber, N., Hector, A., Kuijpers, T., Roos, D. & Hartl, D. Current concepts of hyperinflammation in chronic granulomatous disease. *Clin. Dev. Immunol.* **2012,** 252460 (2012).
31. Winkelstein, J. A. *et al.* Chronic granulomatous disease. Report on a national registry of 368 patients. *Medicine* **79,** 155–169 (2000).
32. Han, W. *et al.* NADPH oxidase limits lipopolysaccharide-induced lung inflammation and injury in mice through reduction-oxidation regulation of NF-κB activity. *J. Immunol.* **190,** 4786–4794 (2013).
33. Wilson, C., Nunez, M. T. & Gonzalez-Billault, C. Contribution of NADPH oxidase to the establishment of hippocampal neuronal polarity in culture. *J. Cell Sci.* **128,** 2989–2995 (2015).
34. Emsley, P. & Cowtan, K. Coot: model-building tools for molecular graphics. *Acta Crystallogr. D* **60,** 2126–2132 (2004).

METHODS

Cell culture. No cell lines used in his study were found in the database of commonly misidentified cell lines that is maintained by ICLAC and NCBI biosample. All of the cell lines were from ATCC or derived from mice as noted below. Cell lines used are identified as macrophages through their gene expression profiles on stimulation to macrophage sub-types. The cell lines were tested for mycoplasma contamination. Quantitative assessment was conducted but data are not included with this version.

RAW 264.7 cells were cultured in RPMI1640 with 10% FBS, 2 mM L-glutamine, 1 mM sodium pyruvate and 55 μM beta-mercaptoethanol. THP-1 cells were cultured in RPMI1640 with 10% FBS, 2 mM L-glutamine and 55 μM beta-mercaptoethanol.

Preparation of mouse primary cells. *Mouse embryonic fibroblasts (MEFs).* Mouse embryos (12.5 to 13.5 days postcoitum; TRE-SCRIB shRNA mice were genotyped by genomic PCR) were dissected into 10 ml PBS. Internal organs from the abdominal cavity were removed and embryos were collected into tubes with 0.5% trypsin/EDTA, and incubated for 30 min in a 37 °C incubator. An equal volume of MEF medium (DMEM with 10% heat-inactivated FBS, 1× non-essential amino acid, 2 mM L-glutamine, and 0.1 mM 2-mercaptoethanol (Invitrogen)) was added to the tubes and centrifuged. The supernatant was removed and pellets were resuspended with fresh MEF media and plated into a 100 mm dish. The Scribble RNAi mice were maintained as per IACUC-approved guidelines.

Bone-marrow-derived dendritic cells (BMDCs). Generation of BMDCs was performed as previously described[35]. In brief, bone marrow was obtained from mouse femurs and tibiae and cultured in RPMI containing 10% FCS and L-glutamine with 40 ng ml^{-1} murine GM-CSF (Peprotech). Fresh medium was added on day 3 and changed on day 6 of culture. Non-adherent dendritic cells were collected on day 8.

Bone-marrow-derived macrophages (BMMs). For BMM, bone marrow was cultured in RPMI with 10% FCS and L-glutamine with 20 ng ml^{-1} murine M-CSF (Peprotech). The culture medium was changed on day 3 of culture and adherent cells were collected on day 6.

Intracellular reactive oxygen species (ROS) detection. *Mouse embryonic fibroblasts.* MEF cells were seeded on a 96-well plate (10^4 cells per well) in complete DMEM medium (see above). After four hours of incubation, the medium was replaced with plain DMEM containing BSA 0.1% for 24 h. The cells were washed with Hank's balanced salt solution (HBSS) and incubated with 100 μM carboxy-H2DCF-DA in DMEM with 0.1% BSA for 30 min. The cells were washed with HBSS to remove carboxy-H2DCF-DA and this was replaced with 0.1 ml of HBSS containing 100 ng ml^{-1} platelet-derived growth factor (PDGF) for 10 min. The signal was measured using a fluorimeter at 490 nm excitation and 538 nm emission.

RAW 264.7 or BMM cells. Cells were seeded at 3×10^5 cells ml^{-1} in a 6-well plate. Dihydroethidium (DHE; Invitrogen) was added to the medium to a final concentration at 5 μM for 30 min in the dark at 37 °C. Cells were washed with HBSS to remove excess DHE. Culture medium containing PMA (1.0 μM) or LPS (100 ng ml^{-1}) was used to stimulate the cells for the indicated time points. The cells were pelleted and resuspended in 200 μl PBS containing 5% FBS and analysed by flow cytometry. DHE appears as red fluorescence.

***In vivo* reactive oxygen species (ROS) detection.** Mice were intraperitoneally injected with 2 mg kg^{-1} LPS (Sigma). Five hours after LPS challenge, the mice were intraperitoneally injected with 25 mg kg^{-1} L-012 (Wako Pure Chemical Industry). Images were taken immediately using a Xenogen IVIS imaging system for 30 min at one minute intervals. Quantitation of the luminescence signal intensity was performed using Living Image software.

Bacterial strains and culture conditions. *Staphylococcus aureus* was purchased from American Type Culture Collection (ATCC) (53657) and cultured in brain–heart infusion agar/broth (ATCC).

Mouse blood bacteria killing assay. *Staphylococcus aureus* were cultured overnight. The *S. aureus* were grown to log phase ($D_{600\,nm}$ between 0.4–0.6). Two hundred millilitres of mouse blood from both +Dox and −Dox mice was incubated with 1.5×10^6 *S. aureus*. The blood–bacteria suspension was rotated gently at 37 °C for 20 min to allow phagocytosis of bacteria. Lysostaphin (2.5 μ ml^{-1}) was added to eliminate extracellular bacteria. At 60 min, 10 μl aliquots were lysed in distilled water and plated in triplicate in soft agar and colonies were counted the next day.

***In vivo* peritoneal bacterial clearance assay.** *S. aureus* was cultured as above. Mice were intraperitoneally injected with 2×10^8 *S. aureus*. Mice were euthanized after 6 h. Peritoneal cavities were lavaged with 5 ml PBS. Lung tissues were collected and homogenized. The samples were serially diluted and plated in triplicate in soft agar and colonies were counted the next day.

Mouse neutrophil purification, ROS detection, and bacteria killing. The manufacturer's instructions (Miltenyl Biotec 130-097-658) were followed. In brief, bone marrow was obtained from mouse femurs and tibiae and labelled with a cocktail of biotin-conjugated antibodies against antigens that are not expressed on neutrophil granulocytes, and then incubated with anti-biotin microbeads (magnetic). All cells (including both magnetic-labelled non-neutrophil and unlabelled neutrophils) were applied to the LS columns that were in the magnetic field of a MACS Separator. All of the cells that were labelled with antibodies were stuck in the column. The cells that not been labelled went through the column. These cells were considered as purified neutrophils. The purified neutrophils were then stained with neutrophil-specific surface markers (CD11b and Gr-1; antibody information can be found in Supplementary Table 1) and analysed by flow cytometry checking the purity. Purified neutrophils (10^5) were stained with DHE (Invitrogen) with a final concentration at 5 μM for 30 min in the dark at 37 °C, and cells were washed with HBSS to remove excess DHE. HBSS containing PMA (1.0 μM) was used to stimulate the cells for 30 min. The cells were pelleted and resuspended in 200 μl PBS containing 5% FBS and analysed by flow cytometry. DHE appears as red fluorescence.

Staphylococcus aureus were cultured overnight. The *S. aureus* were grown to log phase ($D_{600\,nm}$ between 0.4–0.6). Mouse purified neutrophils (10^5) from both +Dox and −Dox mice were incubated with 2×10^6 *S. aureus*. The neutrophil–bacteria suspension was rotated gently at 37 °C for 20 min to allow phagocytosis of bacteria. Lysostaphin (2.5 μ ml^{-1}) was added to eliminate extracellular bacteria. At 60 min, 10 μl aliquots were lysed in distilled water and plated in triplicate in soft agar and colonies were counted the next day.

PCR with reverse transcription, and real-time PCR. All PCR assays with reverse transcription were performed by using a SuperScript III First-Strand Synthesis System. Real-time PCR was performed on a 7900HT system. Primers for real-time PCR were ordered from IDT pre-design assay: IL-1β; IL-12β; and Fizz-1 (Primer information can be found in Supplementary Table 2).

Protein expression and purification. Human SCRIB-PDZ1 (residues 725–815), PDZ2 (860–951), PDZ3 (1002–1092) and PDZ4 (1096–1193) were cloned into the NdeI/HindIII sites of a pET28a vector (Novagen). See Supplementary Table 2 for the primer list. The Scribble PDZ (ScrPDZ) proteins were over-expressed using the *Escherichia coli* BL21-CodonPlus (Stratagene) strain. *E. coli* cells were grown to a $D_{600\,nm}$ of 0.4–0.6 in Luria broth, and expression was induced with 0.1 mM isopropyl β-D-thiogalactopyranoside (IPTG); induced cells were grown overnight at 18 °C. Cells were harvested by centrifugation, resuspended in buffer (50 mM Tris-HCl, pH 8.0, 300 mM NaCl, 20 mM imidazole), and sonicated. Following centrifugation, the supernatant was incubated with Ni^{2+}-NTA (Thermo Fisher) and bound protein was eluted using buffer containing 300 mM imidazole. The eluted protein was further purified using either Superdex75 or Superdex200 size-exclusion chromatography (GE Healthcare) in buffer (20 mM Tris-HCl, pH 8.0. 150 mM NaCl, 1 mM dithiothreitol).

The human p22phox C-terminal tail (p22phox tail) (residues 186–195) was cloned into the BamHI/EcoRI sites of a pGEX4T1 vector (GE Healthcare). The GST-p22tail protein was over-expressed in the *E. coli* BL21-CodonPlus (Stratagene) strain. *E. coli* cells were grown to $D_{600\,nm} = 0.6$, and expression was induced with 0.5 mM IPTG; induced cells were grown for 3 h at 37 °C. Cells were harvested by centrifugation, resuspended in buffer (50 mM Tris-HCl pH 8.0, 300 mM NaCl), sonicated and centrifuged. The supernatant was incubated with glutathione resin (GenScript) and bound protein was eluted using buffer containing 20 mM reduced glutathione.

The human p22phox cytoplasmic proteins (residues 131–195 and 131–185) were cloned and expressed in the same way as the p22phox C-terminal tail. Cells were harvested by centrifugation, resuspended in buffer (50 mM Tris-HCl pH 8.0, 300 mM NaCl), sonicated and centrifuged. The supernatant was incubated with glutathione resin (GenScript) and the N-terminal GST tag was removed by thrombin before Superdex75 size-exclusion chromatography. Purified proteins were confirmed by mass spectrometry analysis.

The ^{15}N- and ^{15}N/^{13}C-labelled SCRIB-PDZ4 proteins were expressed in M9 minimal media containing ^{15}N-NH_4Cl as the sole nitrogen source and ^{13}C-glucose as the carbon source. Expression was induced using 0.2 mM IPTG and cells were cultivated after growing overnight at 20 °C. Cells were harvested by centrifugation, resuspended in buffer (50 mM Tris-HCl, pH 7.5, 300 mM NaCl, 20 mM imidazole), and purified as described for unlabelled SCRIB-PDZ4. For the NMR titration and three-dimensional experiments, N-terminal His-tag was removed by thrombin before size-exclusion chromatography. The final size-exclusion chromatography buffer for the NMR samples was 20 mM sodium phosphate pH 6.0, 100 mM NaCl, 1 mM dithiothreitol.

The ^{15}N-labelled ScrPDZ4 mutants were prepared by using the QuickChange method (Stratagene), and verified by DNA sequencing. Mutant proteins were expressed and purified using identical protocols to the wild-type protein.

DOI: 10.1038/ncb3413

NMR spectroscopy. All NMR titration data were collected at 25 °C on a Bruker Avance III 600-MHz spectrometer equipped with a 1.7 mm TCI MicroCryoProbe. Three-dimensional NMR experiments such as CBCA(CO)NH and HNCACB were performed on a Bruker Avance II NMR 800-MHz spectrometer equipped with a 5 mm TCI CryoProbe, to confirm the transferred SCRIB-PDZ4 assignments from BMRB data (BMRB number 10103). All NMR samples were supplemented with 7.5% (v/v) D_2O. NMR titration experiments were performed using synthesized p22phox C-terminal tail peptide (NPIPVTDEVV) (Genscript). The peptide was dissolved in the same buffer (20 mM sodium phosphate pH 6.0. 100 mM NaCl, 1 mM dithiothreitol) and the pH was re-adjusted to within 0.1 pH unit of the PDZ4 buffer. The peptide concentration was determined by amino acid analysis based on the amount of proline residues. In some titration experiments, *N*-acetylglycine ^{15}N (Sigma) was used to confirm that there were no pH effects during the experiments. The spectra were processed with NMRPipe[36] and visualized using NMRView[37] software. The normalized chemical shift changes were calculated using the equation $\Delta\text{Chemical shift} = \sqrt{[(\Delta H)^2+(\Delta N/6.5)^2]}$.

Modelling steps. The docking model for the SCRIB-PDZ4/peptide complex was generated using pymol with the two previously published structures (1UJU.pdb:SCRIB-PDZ4) and (1MFG.pdb: Erbin-ErbB2) as a template. The alignment was done for the SCRIB-PDZ4 polypeptide chain (with N- and C-terminal tag-related sequences deleted) and the ErbB2 peptide chain (EYLGLDVPV), which is subsequently replaced with the p22phox peptide (NPIPVTDEVV) using Coot. The figure was made using Pymol.

Circular dichroism spectroscopy. Circular dichroism spectroscopic data for 1 mg ml^{-1} SCRIB-PDZ4 samples were collected on a Jasco J-815 CD spectrometer (Jasco) using a 0.1-cm path-length cuvette with the scanning speed of 20 nm min^{-1} (1 nm increments) at 20 °C.

Bio-layer interferometry. Binding affinity of SCRIB-PDZ4 toward p22phox was analysed by bio-layer interferometry (BLI) using the Octet 384 system (ForteBio). Binding assays were performed at 27 °C in the assay buffer (20 mM phosphate pH 6.0. 100 mM NaCl, 1 mM dithiothreitol, 0.01% Tween-20, 1 mg ml^{-1} bovine serum albumin) with vibration at 1,000 r.p.m. Streptavidin-coated sensors loaded with biotinylated p22phoxC10 were incubated with the analyte (WT or G1112A/R1178A SCRIB-PDZ4 in a range of 5–20 μM concentration), and subsequently in the assay buffer to generate the association and dissociation binding curves used for kinetic analysis.

His pulldown assay. Freshly made 0.5 μg purified GST-tagged p22phox c-tail and 1 μg HIS-tagged individual PDZ domains from the previous step were diluted in 700 μl CBL and incubated with 5 μl of His beads (Cell Signaling) for 2 h at 4 °C. The beads/resin was washed 3 times with CBL buffer. The resulting precipitants were analysed by immunoblotting with anti-GST (Cell Signaling).

Immunofluorescence staining. Cells were fixed using 4% PFA for 30 min and blocked in PBS containing 0.5% BSA and 0.05% saponin for 60 min. Primary antibodies were diluted in the same blocking buffer and incubated overnight at 4 °C. Secondary antibodies were diluted in the same blocking buffer and incubated with the samples for 60 min. Antibody information can be found in Supplementary Table 1.

Live imaging for *S. aureus* phagocytosis. Thp1 cells were plated on MatTek's Glass Bottom Culture Dishes and stimulated as previously described with 1 mM PMA for 24 h (ref. 38). Live *S. aureus* was conjugated with FITC using the BacLight green bacterial stain kit (Life Technology). 2×10^5 bacterial units were added to the Thp1 cells and immediately imaged using a 60× oil immersion objective (3× field zoom) on a Nikon C2 confocal microscope connected to a Tokai Hit live imaging chamber at the intervals described in the results section for a duration of 2.0 h.

RAW 264.7 cells were plated on MatTek's Glass Bottom Culture Dishes overnight. pHrodo-red *S. aureus* bioparticles (5×10^5; Life Technology) were added to the RAW 264.7 cells and immediately imaged using a 60× oil immersion objective (3× field zoom) on a Nikon C2 confocal microscope connected to a Tokai Hit live imaging chamber at the intervals described in the results section for a duration of 1.0 h.

Immunogold labelling for transmission electron microscopy. RAW 264.7 Luc shRNA or SCRIB shRNA cells were incubated with *S. aureus* for 60 min. Samples were fixed in 0.2% glutaraldehyde with 4% paraformaldehyde at room temperature for one hour, embedded and sectioned. The section grids were blocked for 2.0 h in conditioned TBS (100 mM Tris-buffered saline (pH 7.0), 1 mM $CaCl_2$, 1 mM $MgCl_2$, 0.1% globulin-free BSA, 0.4% cold-water fish gelatin) and incubated with anti-SCRIB antibody diluted 1:100 in conditioned TBS. The grids were incubated with secondary antibody conjugated with 10 nm gold particles (antibody information can be found in Supplementary Table 1; Electron Microscopy Sciences) for 1.0 h at room temperature. Grids were counter-stained with saturated uranyl acetate for 15 s and then the sections were examined and photographed in a Hitachi H7000 transmission electron microscope at an accelerating voltage of 75 kV.

Cerium perhydroxide precipitate in phagosomes. The assay was performed following the protocol described previously[22]. In brief, 10^5 RAW 264.7 cells were infected with 10^6 *S. aureus* for 60 min, and cells were washed with 0.1M Tris maleate buffer (pH 7.5), followed by the addition of 0.1 M Tris maleate, 7% sucrose, 1 mM aminotriazole buffer (pH 7.5) for 10 min at 37 °C. Next, cells were treated with 0.1 M Tris maleate, 7% sucrose, 1 mM aminotriazole, 1 mM $CeCl_3$, 0.71 mM NADH, 0.71 mM NADPH buffer (pH 7.5) for 20 min at 37 °C. The sample was fixed in 2.5% glutaraldehyde and analysed by transmission electron microscopy.

Immunoprecipitation and immunoblotting. Cells were lysed and analysed using previously established protocols[4]. Antibodies used: for immunoprecipitation, 500 μg protein was incubated with 20μl protein A beads (Sigma) and 4 μg of primary antibody, or with 20 μl Flag-resin (Sigma), or with 10 μl Myc-resin (Cell Signaling) overnight at 4 °C with gentle agitation. Antibodies used for immunoblotting: SCRIB, phosphor-PDGFR (Tyr857), PDGFR-beta, anti-myc, anti-p47phox, anti-flag, anti-p22phox, anti-gp91, anti-p67phox and anti-p40phox. Antibody information can be found in Supplementary Table 1.

Retroviral/lentiviral microRNA-based RNA interference and plasmid construction. RNA interference vectors targeting expression of Scribble were designed as previously described[4]. In brief, a 97-nucleotide oligonucleotide was synthesized that has a 5′ miR30 flanking sequence, a sense strand Scribble target sequence, a common miR30 loop sequence, an antisense strand targeting Scribble, and a common 3′miR30 flanking sequence. RNAi sequence information can be found in Supplementary Table 2. The sequence was amplified using polymerase chain reaction (PCR) primers that recognize the miR30 flanking sequence and have Xho1 and EcoR1 restriction enzyme sites. The PCR product was subcloned into a MSCV LTR hygromycin vector.

Flow cytometry and antibodies. BMMs were stained with monoclonal antibodies specific for CD11b and F4/80 (eBioscience) and analysed by flow cytometry. Antibody information can be found in Supplementary Table 1. Unstimulated BMDCs were stained with CD11b and CD11c and BMDCs stimulated with LPS or CpG ODN 1826 (Integrated DNA Technologies) for 16 h were stained with CD80, CD86 (eBioscience), CD40, (BD Biosciences), and MHCII (Biolegend). Flow cytometry data were acquired on a BD FACSCanto II (Becton Dickinson) and analysed with FlowJo software (Treestar).

Chromatin immunoprecipitation. The manufacturer's instructions were followed (Sigma CHP1). In brief, cells were fixed and crosslinked by formaldehyde and nuclear DNA was broken into small fragment by sonication. ChIP-grade p65 (Abcam) antibody was used for immunoprecipitation Antibody information can be found in Supplementary Table 1. Primer information for IL-6 and TNF promoters can be found in Supplementary Table 2.

Animal model. The mice used in the manuscripts were FVB.TRE.ScribRNAi mice; 8–12 weeks old, male. In each experiment, a minimum of 3 mice from each group were used (see Figs 1f,i and 4b–d and 5c–e figure legend for detail).

The procedures were approved by the University Health Network animal safety committee.

Animal experiments. No statistical method was used to predetermine sample size. The experiments were not randomized. The investigators were not blinded to allocation during experiments and outcome assessment.

Statistics and reproducibility. All of the statistical analyses were two-tailed, unpaired, *t*-tests with equal variances. All of the experiments were repeated three times unless stated otherwise. All of the experiments were repeated three independent times with similar results. Images shown are representative of the images obtained.

Data availability. NMR data supporting the findings in Fig. 3b and Supplementary Fig. 3b,c,g,i can be accessed from the BMRB repository under BMRB accession numbers: 26863 and 26864. Source data for Fig. 3g are provided in Supplementary Table 3. All data (both NMR and others) supporting the findings of this study are available from the authors on request.

35. Lutz, M. B. *et al.* An advanced culture method for generating large quantities of highly pure dendritic cells from mouse bone marrow. *J. Immunol. Methods* **223,** 77–92 (1999).
36. Delaglio, F. *et al.* NMRPipe: a multidimensional spectral processing system based on UNIX pipes. *J. Biomol. NMR* **6,** 277–293 (1995).
37. Johnson, B. A. & Blevins, R. A. NMR View: A computer program for the visualization and analysis of NMR data. *J. Biomol. NMR* **4,** 603–614 (1994).
38. Tsuchiya, S. *et al.* Induction of maturation in cultured human monocytic leukemia cells by a phorbol diester. *Cancer Res.* **42,** 1530–1536 (1982).

nature cell biology

DOI: 10.1038/ncb3413

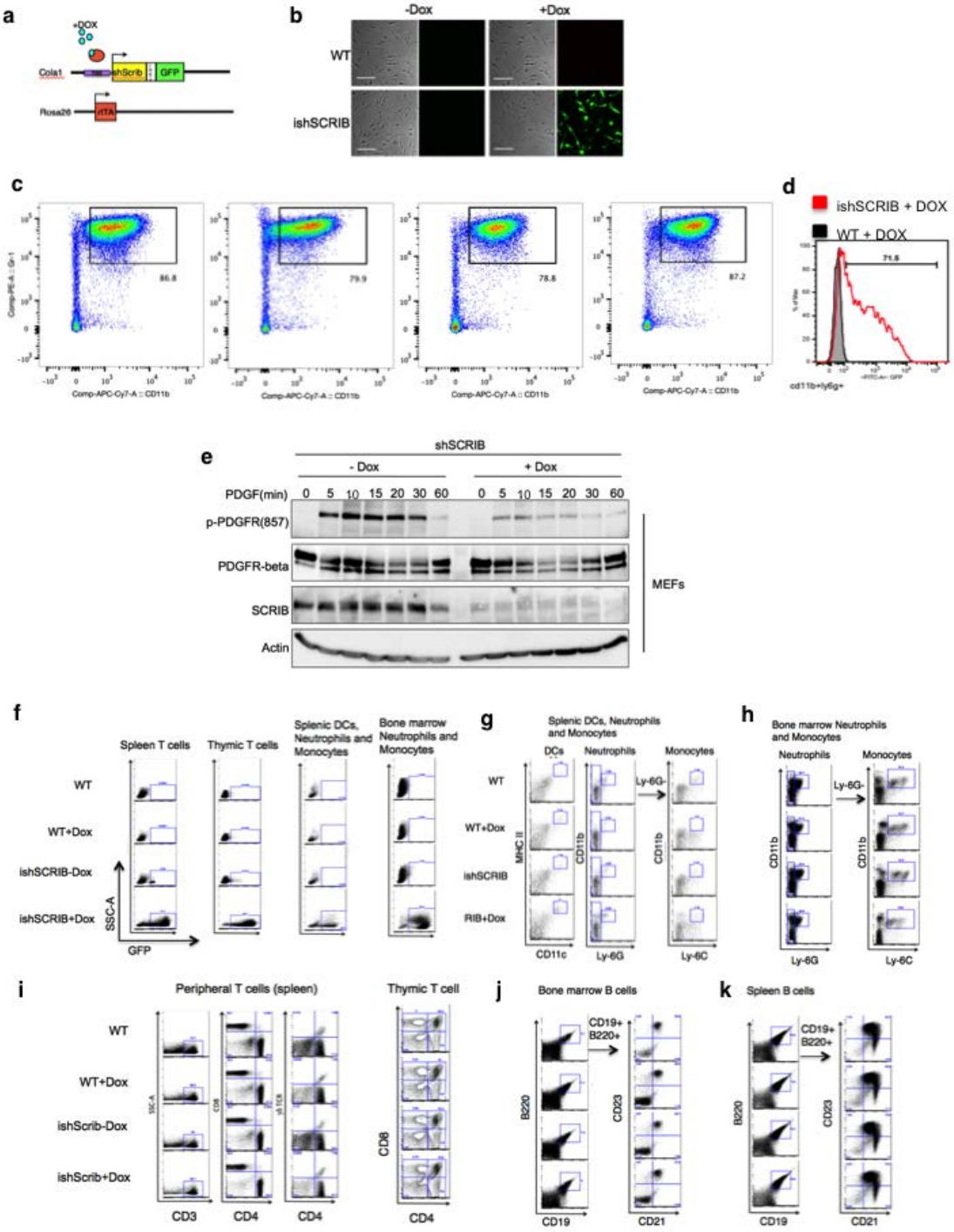

Supplementary Figure 1 SCRIB is required for reactive oxygen species (ROS) generation. **(a)** Schematic diagram of the tetracycline-inducible knock-in constructs used to generate SCRIB shRNA mice. **(b)** Bone marrow derived macrophages were imaged with confocal microscope. Representative images are shown. Scale bar represents 50 ㎜.. Bone marrow cells were isolated from WT+Dox or -Dox, ishSCRIB+Dox or -Dox mice, and then neutrophils were isolated. Cells were then stained for flow cytometry and analyzed by flow cytometry checking the purity of neutrophils **(c)**, or the expression of ishSCRIB (GFP) **(d)**. **(e)** Immunoblot analysis of PDGF (50 ng/ml) induced PDGFR-β tyrosine phosphorylation in MEFs at indicated time points. Immune cells isolated from bone marrow, spleen, thymus from WT and ishSCRIB mice (8 to 12 weeks old) with normal food or Dox food were analyzed GFP signal **(f)**, Splenic cells stained with indicated surface marker for dendritic cells, neutrophils, and monocytes **(g)**; bone marrow cells stained with surface marker for neutrophils, and monocytes **(h)**; splenic cells and thymic cells were stained with T cell surface maker **(i)**; bone marrow cells stained with B cell surface marker **(j)**; and splenic cells stained with B cell surface maker **(k)**.

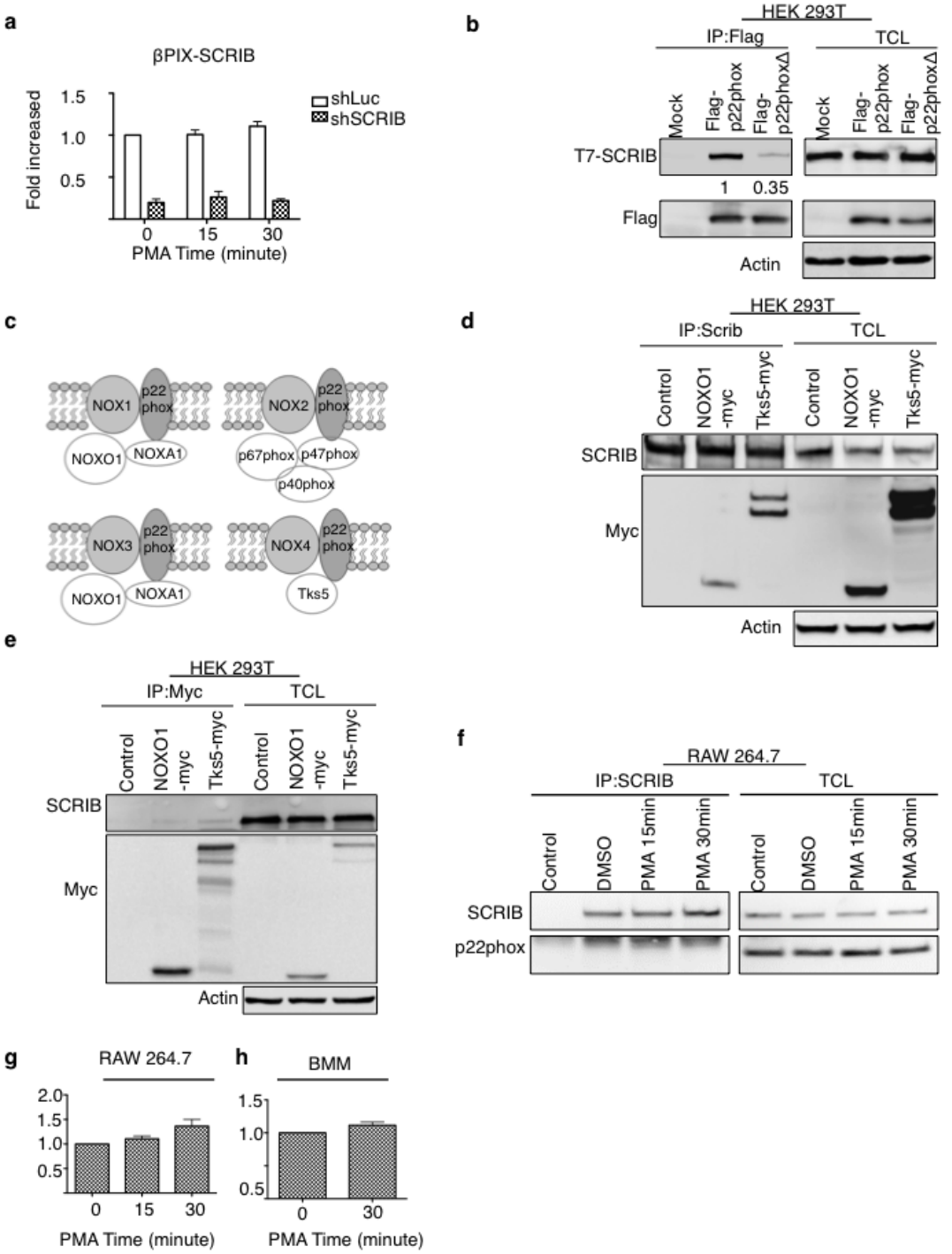

Supplementary Figure 2 SCRIB is a component of the NOX complex. **(a)** Quantitation of SCRIB binding to β-PIX. **(b)** Wild type (WT), Flagp22phox (Flag-p22) or Flag-p22phox without last four amino acid (Flag-p22Δ) were co-transfected with T7 tagged full length SCRIB. Flag immunoprecipitants were recovered and analyzed by anti-Flag and anti-T7 immunoblots. n=3 biologically independent experiments (mean ± SD). (two-tailed, unpaired t-test with equal variances: p=0.001). **(c)** Components of the four NOX complexes, NOX1-4. **(d)** Total cell lysates (TCL) from 293T cells transfected with Myc-tagged NOX complex proteins or anti-Myc immunoprecipitates were analyzed for the presence of endogenous SCRIB. **(e)** Total cell lysates (TCL) from 293T cells transfected with Myc-tagged NOX complex proteins or anti-Myc immunoprecipitates were analyzed for the presence of Myc-tagged proteins. **(f)** SCRIB immunoprecipitation followed by anti p22phox immunoblots using lysates obtained from parental RAW 264.7 cell line. Quantitation of p22phox binding to SCRIB in RAW 264.7 cell line **(g)** or in bone marrow derived macrophages **(h)** stimulated with PMA. Each experiment was performed in triplicate and data presented is an average of n=3 independent experiments (mean ± SD). Unprocessed scans of full blots/gels are shown in Supplementary Figure 6.

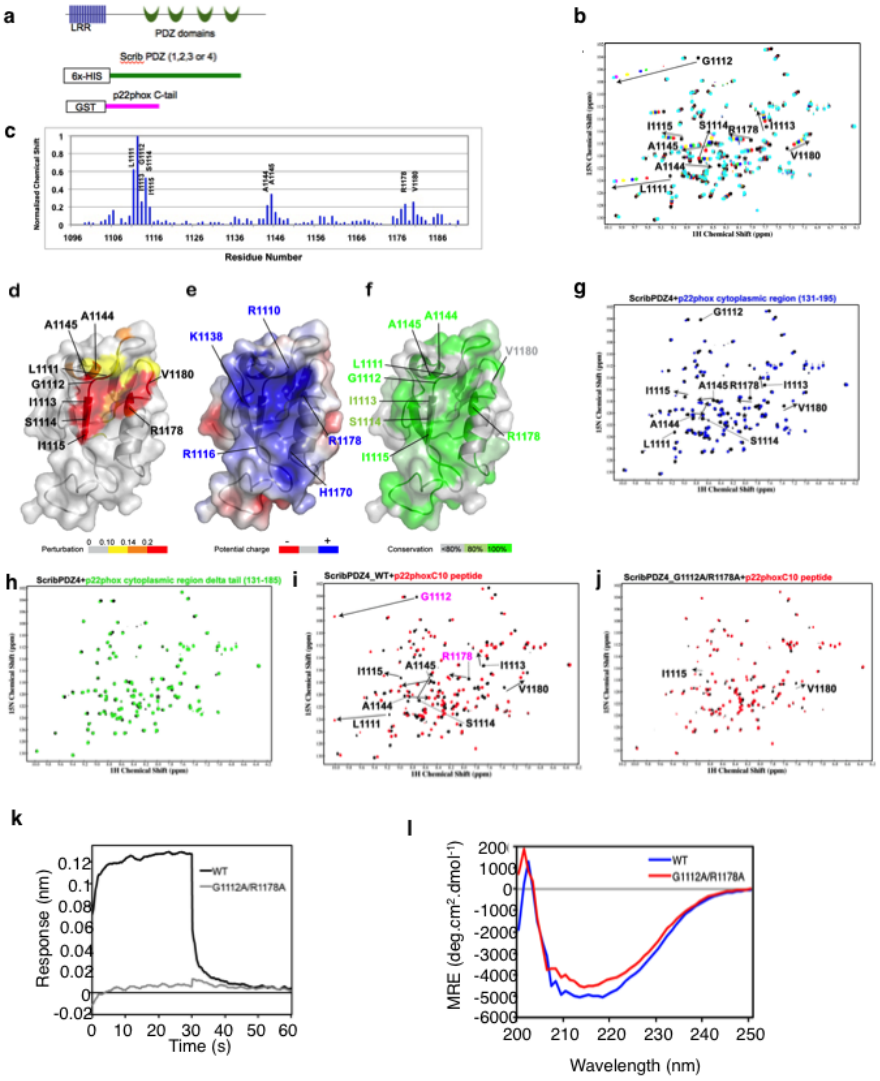

Supplementary Figure 3 SCRIB interacts directly with p22phox, which is required for PMA-induced generation of ROS. **(a)** Schematic showing the full length SCRIB protein with Leucine Rich Repeats (LRR) and PDZ domains and the 6xHIS-tagged individual SCRIB PDZ domains or GST-tagged p22phox C-terminal tail (GST-p22tail). **(b)** ^{1}H-^{15}N heteronuclear single quantum coherence (HSQC) spectrum of ^{15}N- labeled ScrPDZ4 (0.2 mM) in the absence (black) and the presence of varying concentration ratio of p22phox tail peptide/SCRIBPDZ4: 1.5 (red), 3.0 (green), 4.5 (blue), 8.9 (yellow), 17.8 (magenta) and 26.7-fold (cyan), are shown. Assignments were transferred from human SCRIB PDZ4 domain (BMRB number 10103) and further confirmed by 3D NMR experiments. Residues exhibiting large chemical shift (>0.2 normalized chemical shift change in Figure S3C) are indicated. An asterisk (*) indicates the peak from N-Acetylglycine-^{15}N. Repeated 4 times and the representative experiment was shown as a figure. **(c)** NMR characterization of the interaction between p22phox tail and His-SCRIBPDZ4. The chemical shift change of each SCRIBPDZ4 residue is normalized to the observed change for G1112 in the presence of the p22phox tail peptide (26.7-fold). Blank regions indicate residues for which the value cannot be determined because of overlapped or unassigned peaks. Residues exhibiting large chemical shifts (>0.2 normalized chemical shift change) are labeled. **(d)** SCRIBPDZ4 residues affected by the addition of p22phox tail peptide are mapped and indicated on the apo SCRIBPDZ4 structure (i.e. residues 8-105 from PDB ID 1UJU). **(e)** Electrostatic potential surface representation of SCRIBPDZ4 at neutral pH. Basic and acidic potentials are shown in blue (+5 kT/e) and red (-5 kT/e), respectively. Basic residues near p22phox binding pocket are indicated. The electrostatic surface potential was generated using the APBS tools in Pymol, with partial charges determined by the PDB2PQR server (http://nbcr-222.ucsd.edu/pdb2pqr_1.8/). **(f)** Conservation of SCRIBPDZ4 residues. Percent conservation of each residue position in human SCRIBPDZ4 (Residues within R1099-C1189) compared to the alignment of mouse, rat, zebrafish and fly SCRIB PDZ4 protein sequences. The residues affected by p22phox tail binding are shown. **(g)** ^{1}H-^{15}N HSQC spectrum of ^{15}N-labeled ScrPDZ4 (0.2mM) in the absence (black) and the presence (blue) of the full p22phox cytoplasmic region (i.e. residues 131-195, 5.0-fold excess). Residues exhibiting large chemical shift in Figure S2 are indicated. Repeated twice and the representative experiment was shown as a figure. **(h)** ^{1}H-^{15}N HSQC spectrum of ^{15}N-labeled SCRIBPDZ4 (0.2 mM) in the absence (black) and the presence (green) of the p22phox cytoplasmic region with a C-terminal tail truncation (i.e. residues 131-185, 5.0- fold excess). An asterisk (*) indicates peaks from N-Acetylglicine-^{15}N. Repeated twice and the representative experiment was shown as a figure. HSQC spectra of wild-type **(i)** and G1112A/R1178A double mutant **(j)** ^{15}N-labeled ScrPDZ4 (0.1 mM) in the absence (black) and the presence (red) of p22phox tail peptide (32.4-fold) are shown. Repeated twice and the representative experiment was shown as a figure. **(k)** CD spectra of the wild type (WT) and G1112A/R1178A double mutant forms of Scrib-PDZ4. (l) Comparison of response curves of WT and G1112A/R1178A variants of ScribPDZ4. Response curve was obtained with 20 μM ScribPDZ4 proteins.

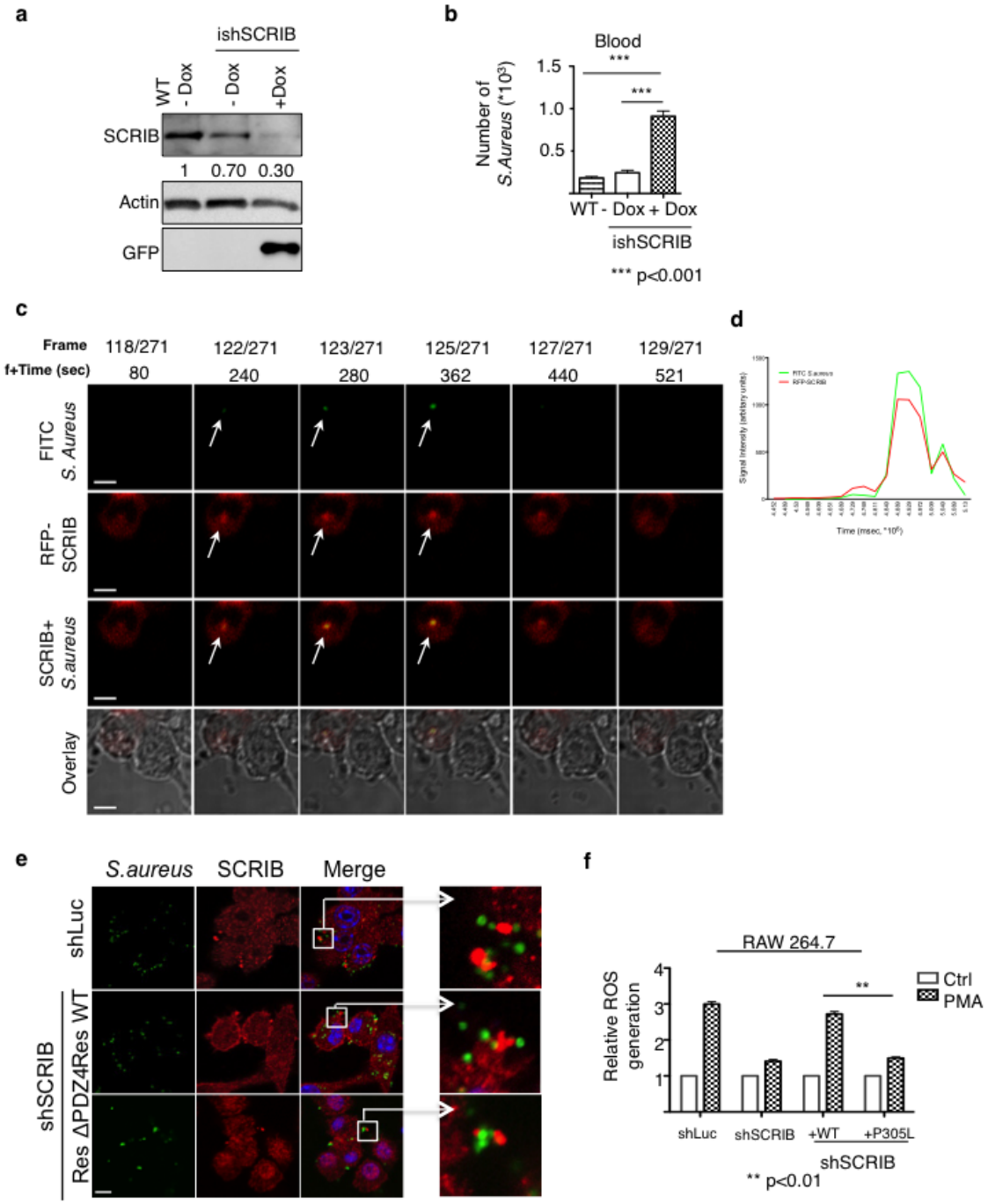

Supplementary Figure 4 SCRIB required for clearing *S. aureus* infection *in vivo* and is recruited to phagosomes to mediate production of ROS. **(a)** Immunoblot analysis for SCRIB and GFP expression in whole blood from WT, ishSCRIB mice. **(b)** Whole blood from WT, ishSCRIB+Dox or -Dox mice was incubated with *S.aureus* for 20 minutes. Lysotaphin was added at 20 minutes of incubation and aliquots were removed at 60 minutes for enumeration of *S.aureus* CFU. Blood from n=3 independent mice were used and error bar represents mean ± SD. (two-tailed, unpaired t-test with equal variances: p=0.001. (c) Cells were imaged every 40 seconds for 2.0 hours. FITC containing phagosomes were detected at f+80 seconds (where f is frame 116 out of 271, an arbitrary frame chosen that precedes observation of phagocytic events after addition of *S. aureus*). Concomitant accumulation of RFP-SCRIB around the FITC-*S. aureus* (t=480 sec) intensity that localized to and around the site of bacterial engulfment as monitored with the FITC *S. aureus* signal, white arrow. Scale bar is 5μm. **(d)** Quantification of FITC *S.aureus* (green line) and RFP-SCRIB (red line) signal intensity at the point of phagocytosis that correlates with the time frames shown in **(c)**. Increases in RFP-SCRIB intensity largely follow the same pattern and colocalize with FITC *S.aureus* at the time of phagocytosis. **(e)** Cells were incubated with phrodo-*S. aureus* for 1 hour and then fixed for immunofluorescence staining. Representative and magnified inset images are shown. Green is *pHrodo-S. aureus*; red is SCRIB. Scale bar is 5μm. **(f)** RAW 264.7shSCRIB cells lacking endogenous SCRIB were used to re-express wild type SCRIB (WT.Rescue), or with SCRIB with point mutation in the LRR domain (P305L) (P305L.Rescue). n=3 biologically independent experiments (mean ± SD). (two-tailed, unpaired t-test with equal variances: p=0.01). Unprocessed scans of full blots/gels are shown in Supplementary Figure 6.

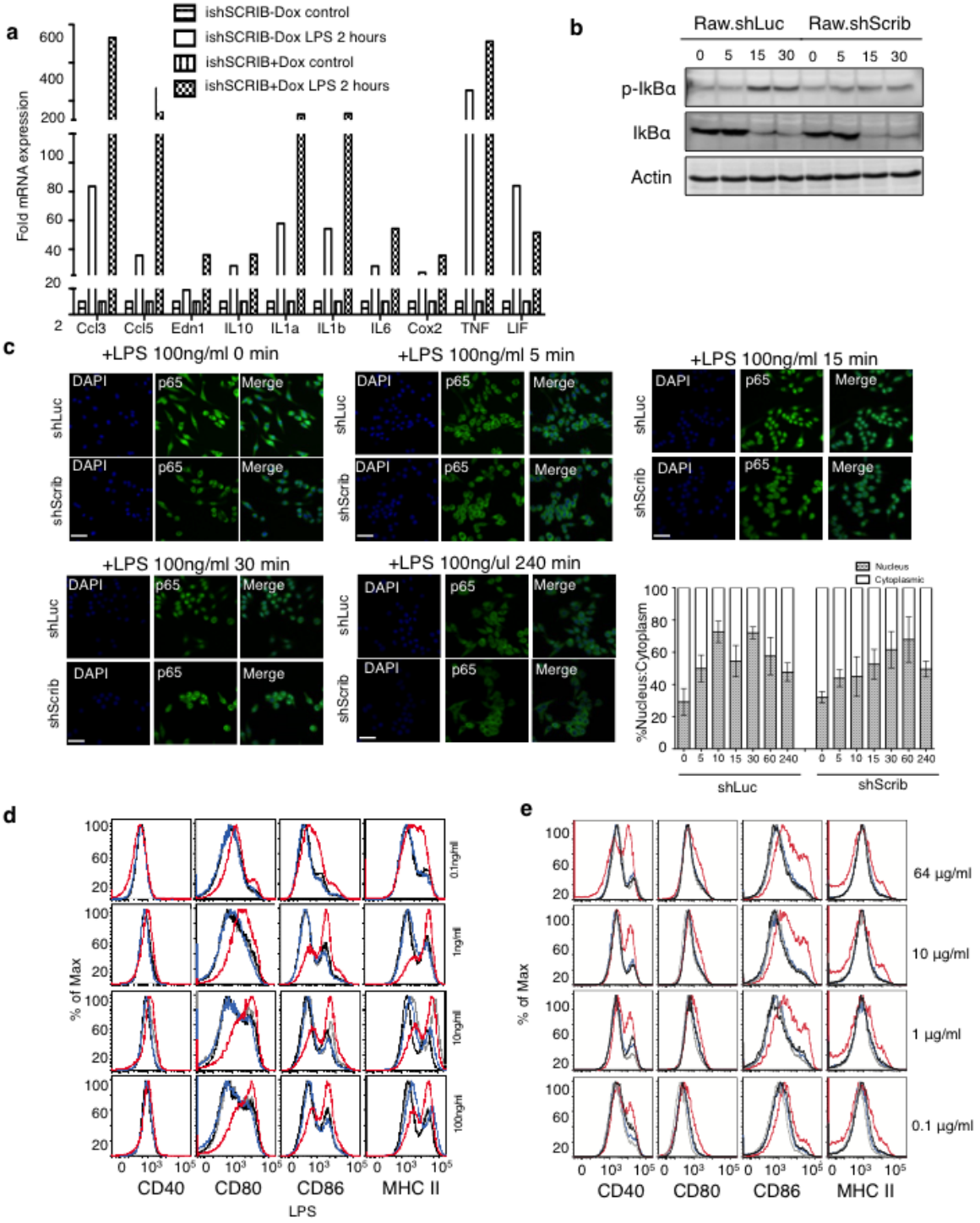

Supplementary Figure 5 SCRIB regulated inflammatory response. **(a)** Bone marrow cells were isolated from ishSCRIB mice with normal food. Cells were split into two groups: in present of Doxycycline (1µg/ml) or not in present of Doxycycline. After 7 day of culture, cells were treated with LPS (100ng/ml) for 2.0 hours. RNA were isolated from untreated cells and treated cells and then followed by reverse transcripts PCRs. cDNA were used for Taqman array mouse inflammation gene set. Data shown is average of results from 2 mice. **(b)** Lysates from RAW 264.7shLuc (control) or shScrib treated with LPS (100 ng/ml) for indicated time point, immunoblotted for p-IkBα, IkBα, and Actin. **(c)** Confocal microscope images of RAW264.7 cells before or after stimulated with LPS for 5 minutes, 15 minutes, 30 minutes or 3 hours, fixed and stained for p65 (green) and DAPI (blue). Representative images were shown on the left panel (scale bars represent 50 µm) and quantification of p65 translocate to the nuclear were shown on the bottom right panel. n=3 biologically independent experiments (mean ± SD). (two-tailed, unpaired t-test with equal variances: p=0.01). BMDCs from WT or ishSCRIB mice were grown as described in Methods with or without Dox. On day 8, DCs were harvested and stimulated with LPS **(d)** or CpG **(e)** for 18h at the concentrations indicated. Data shown is representative of reproducible results from 2 mice **(d)** DC cells were then stained for indicated markers and analyzed by flow cytometry. Unprocessed scans of full blots/gels are shown in Supplementary Figure 6.

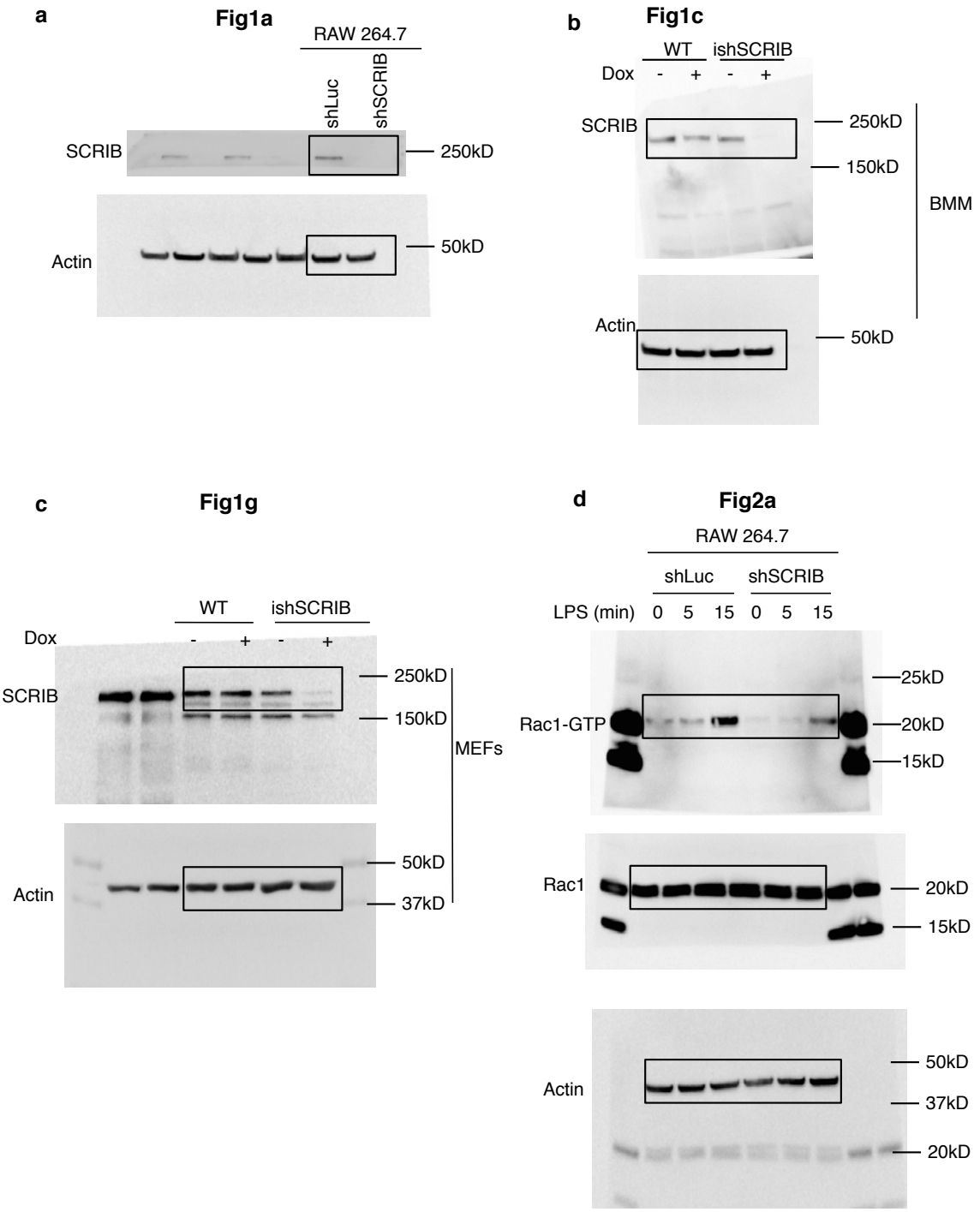

Supplementary Figure 6 Unprocessed blots/gel employed in the current manuscript.

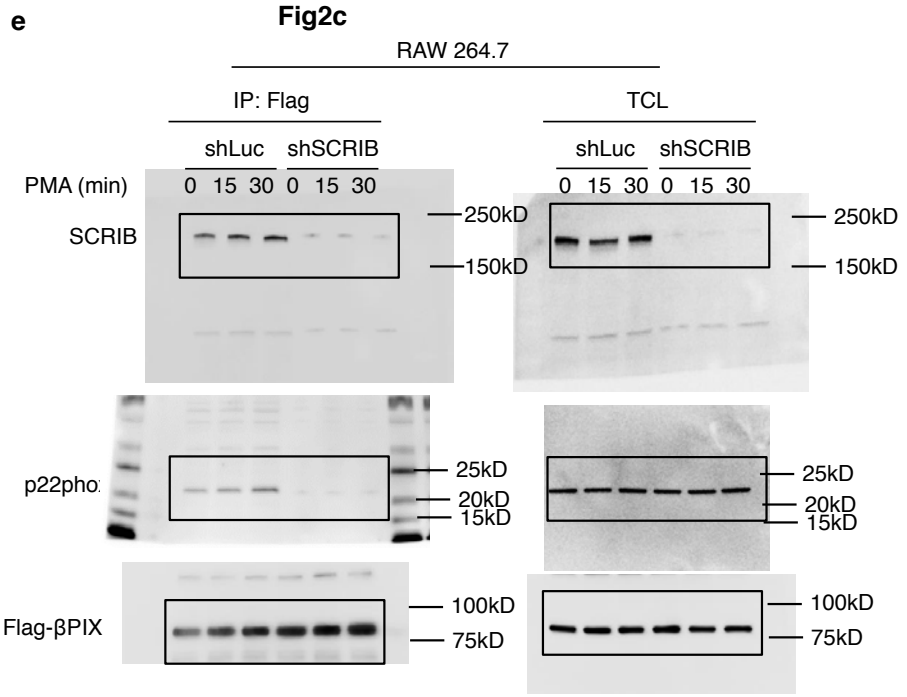

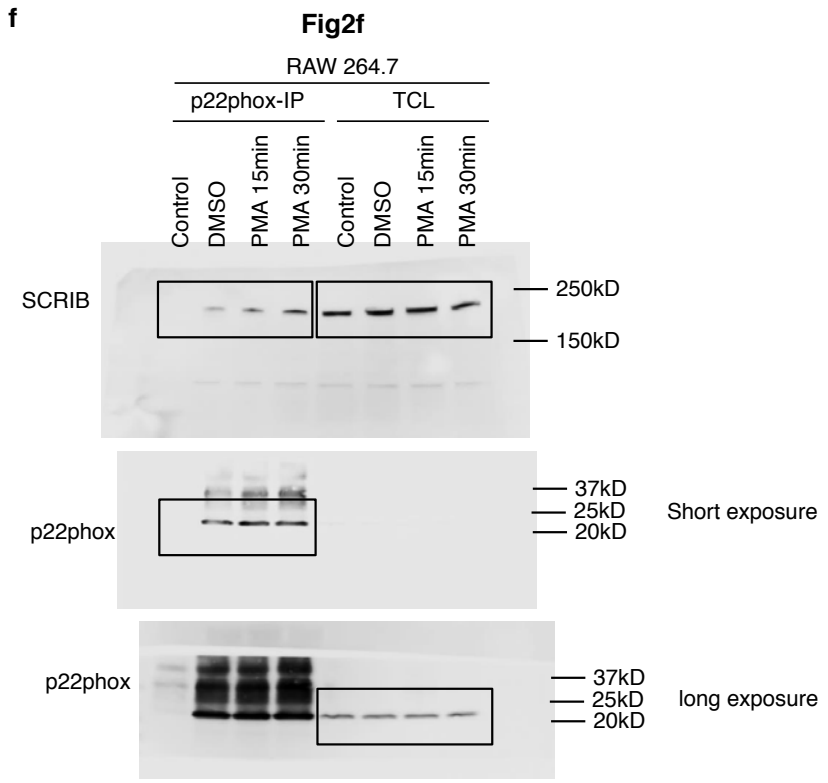

Supplementary Figure 6 continued

g

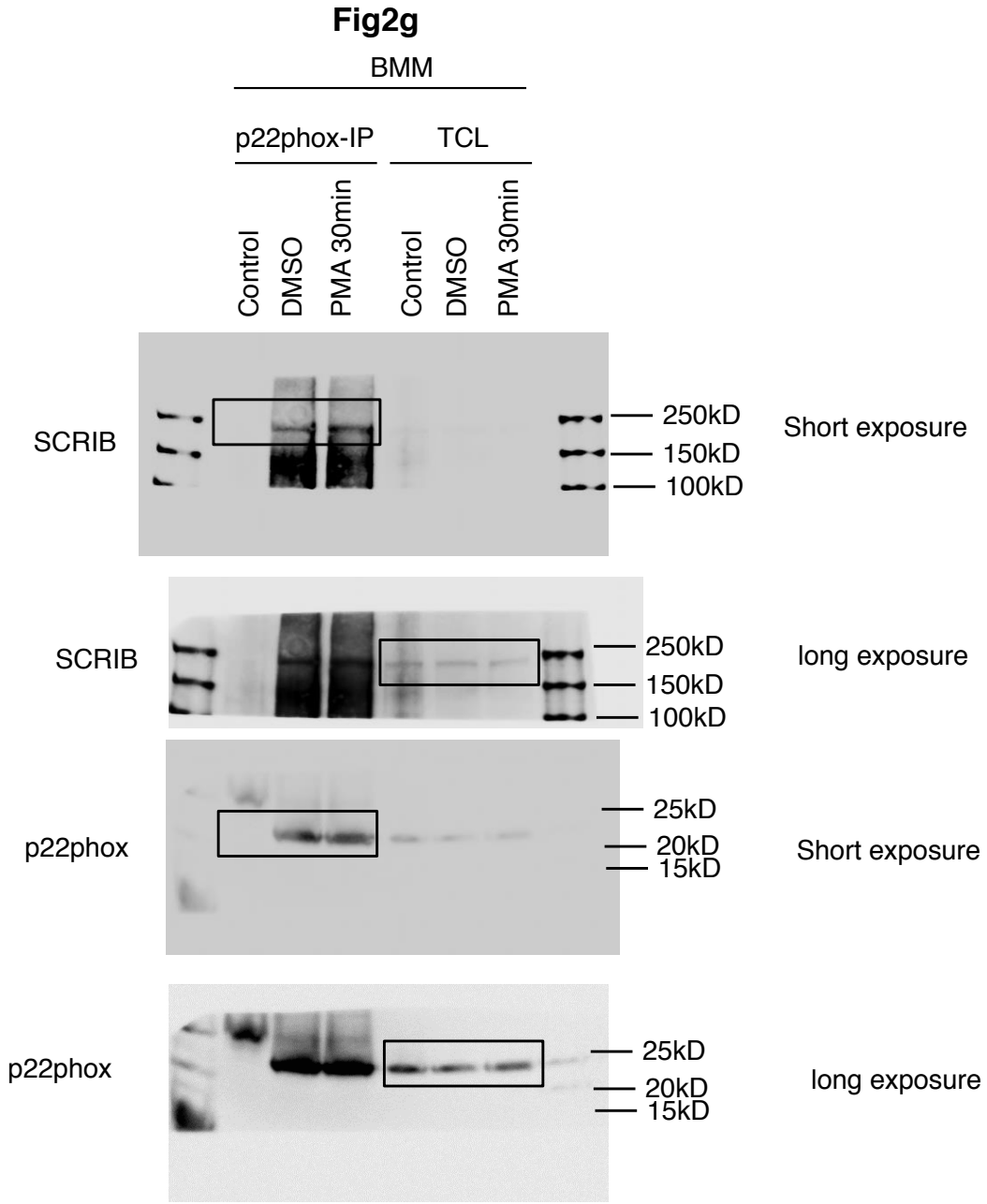

Supplementary Figure 6 continued

h

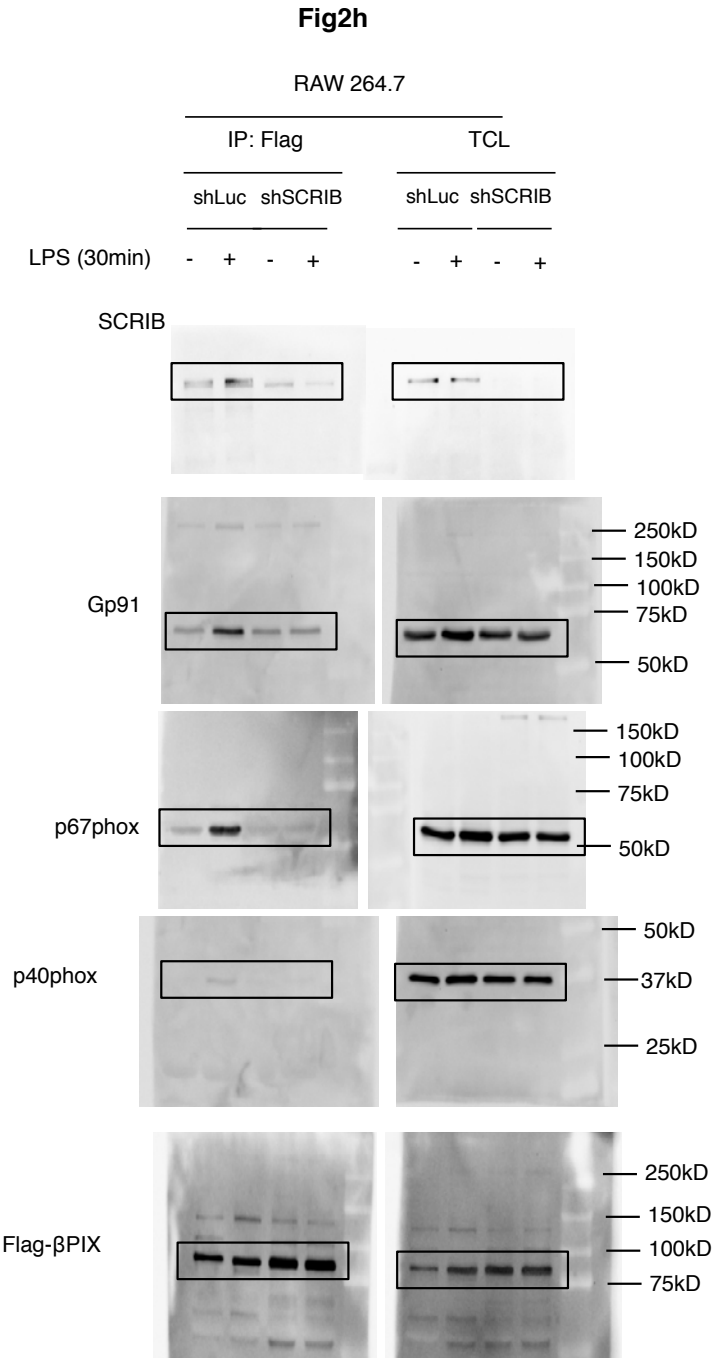

Supplementary Figure 6 continued

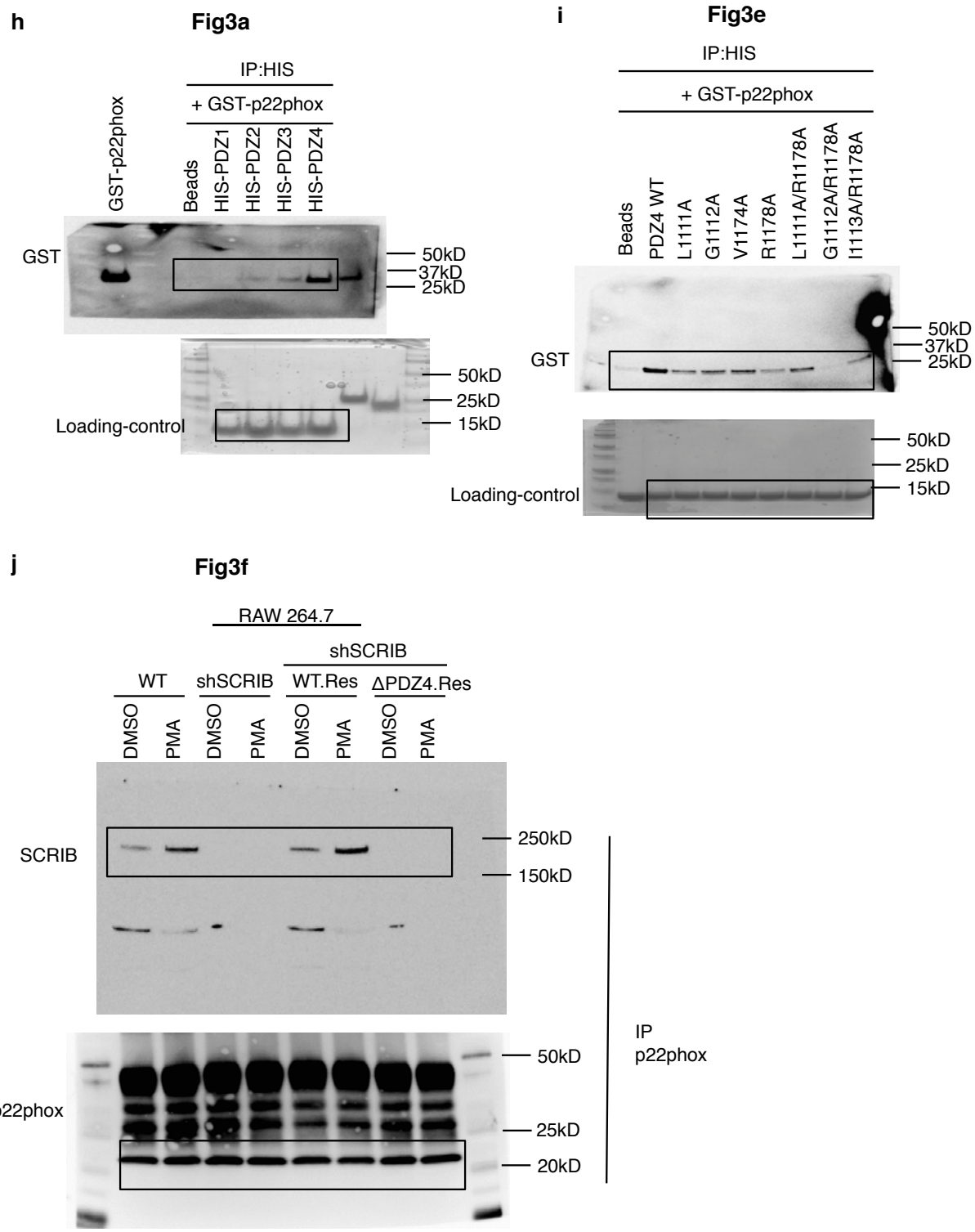

Supplementary Figure 6 continued

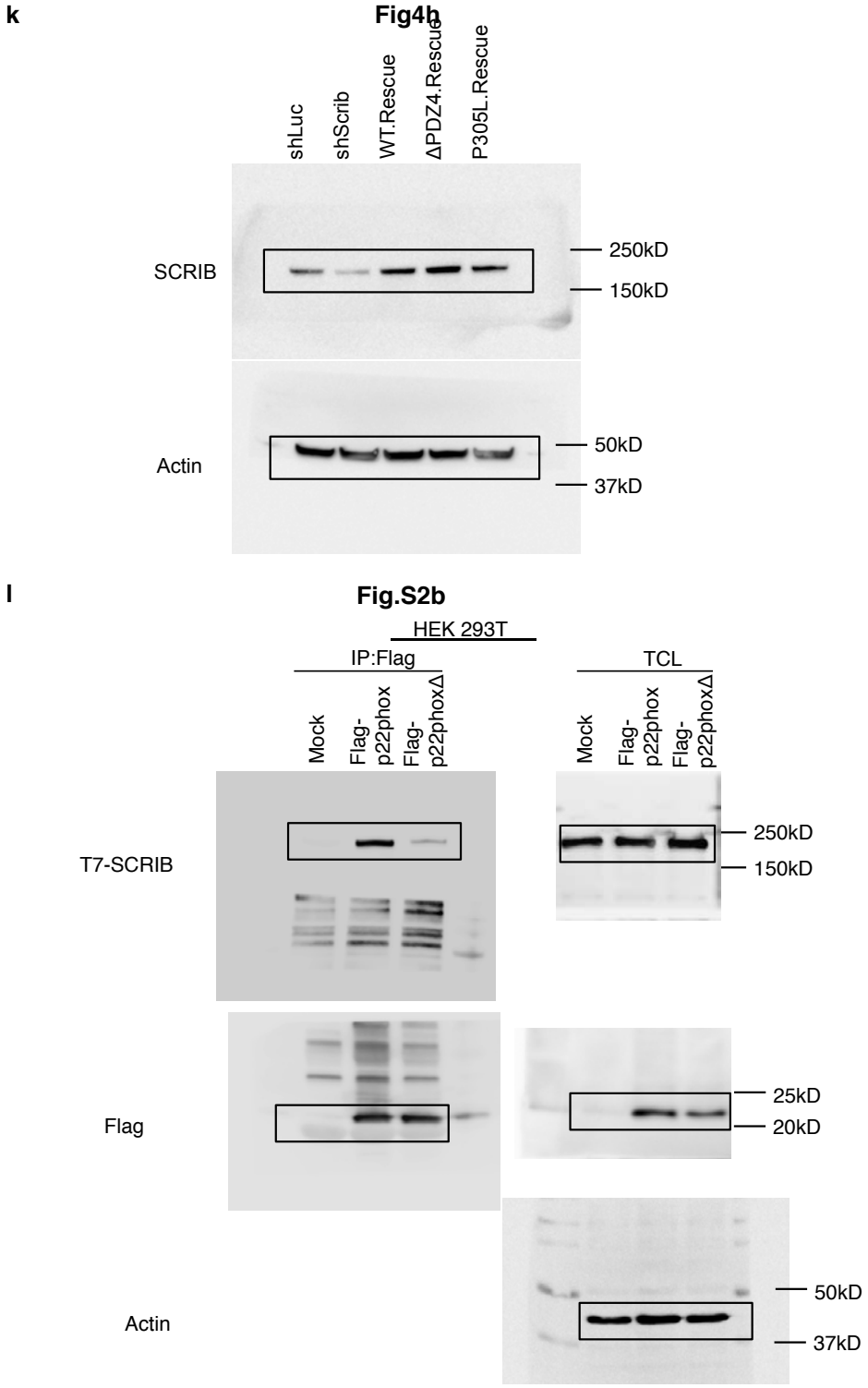

Supplementary Figure 6 continued

m

Fig.S2d

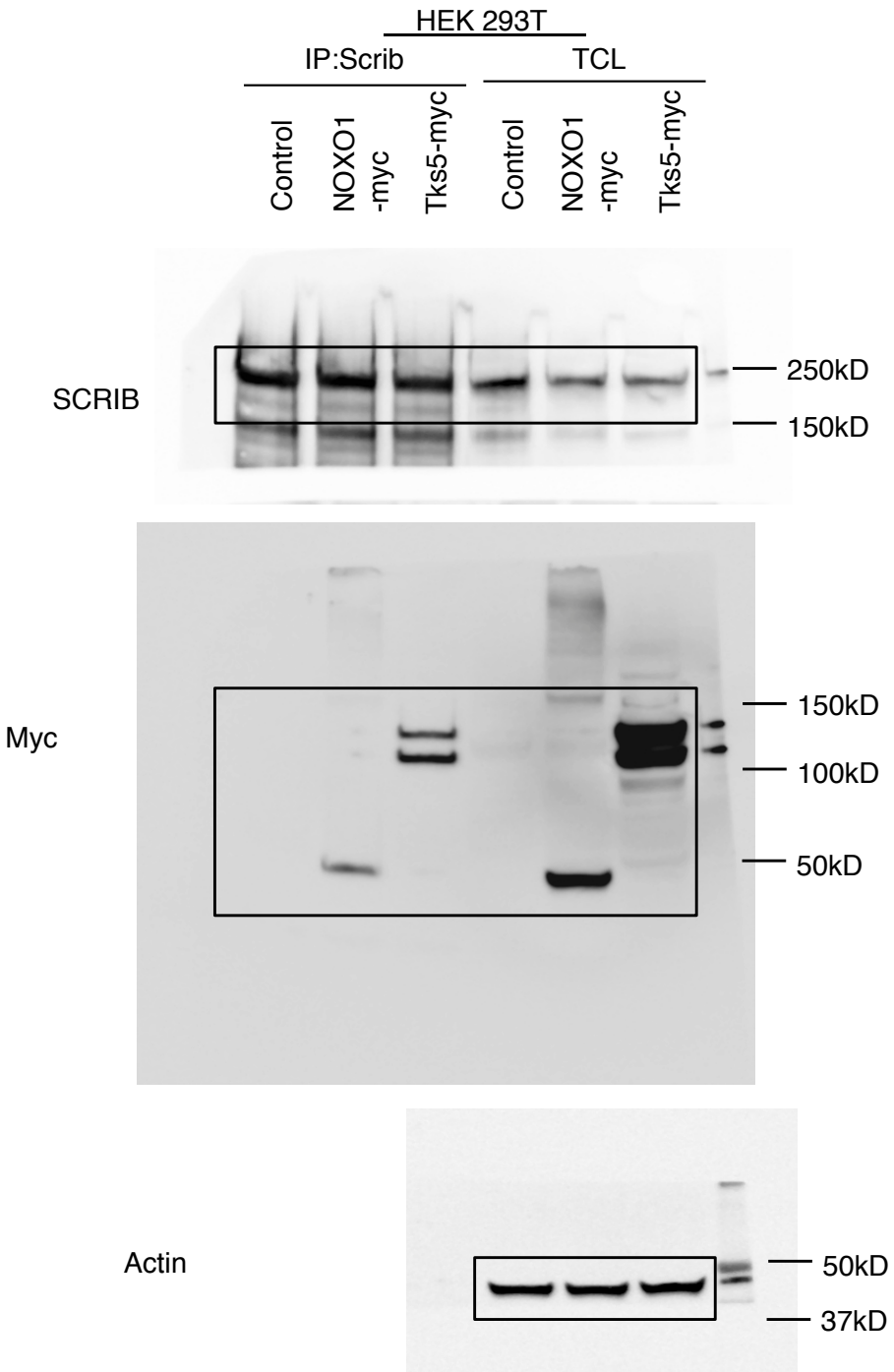

Supplementary Figure 6 continued

n

Fig.S2e

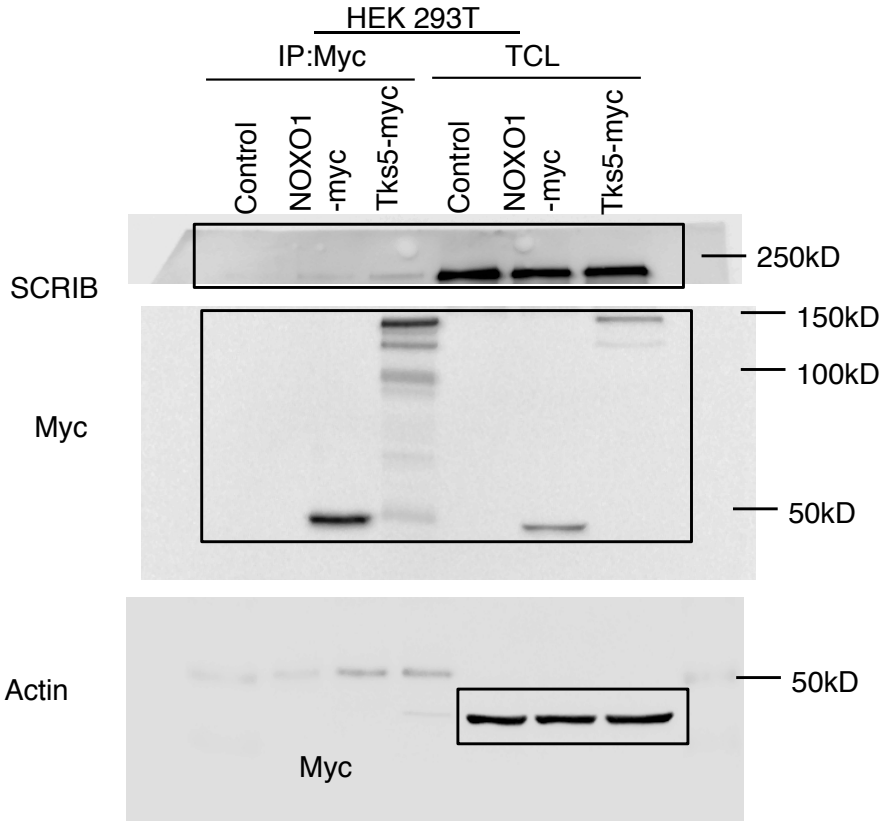

Supplementary Figure 6 continued

o

Fig.S2f

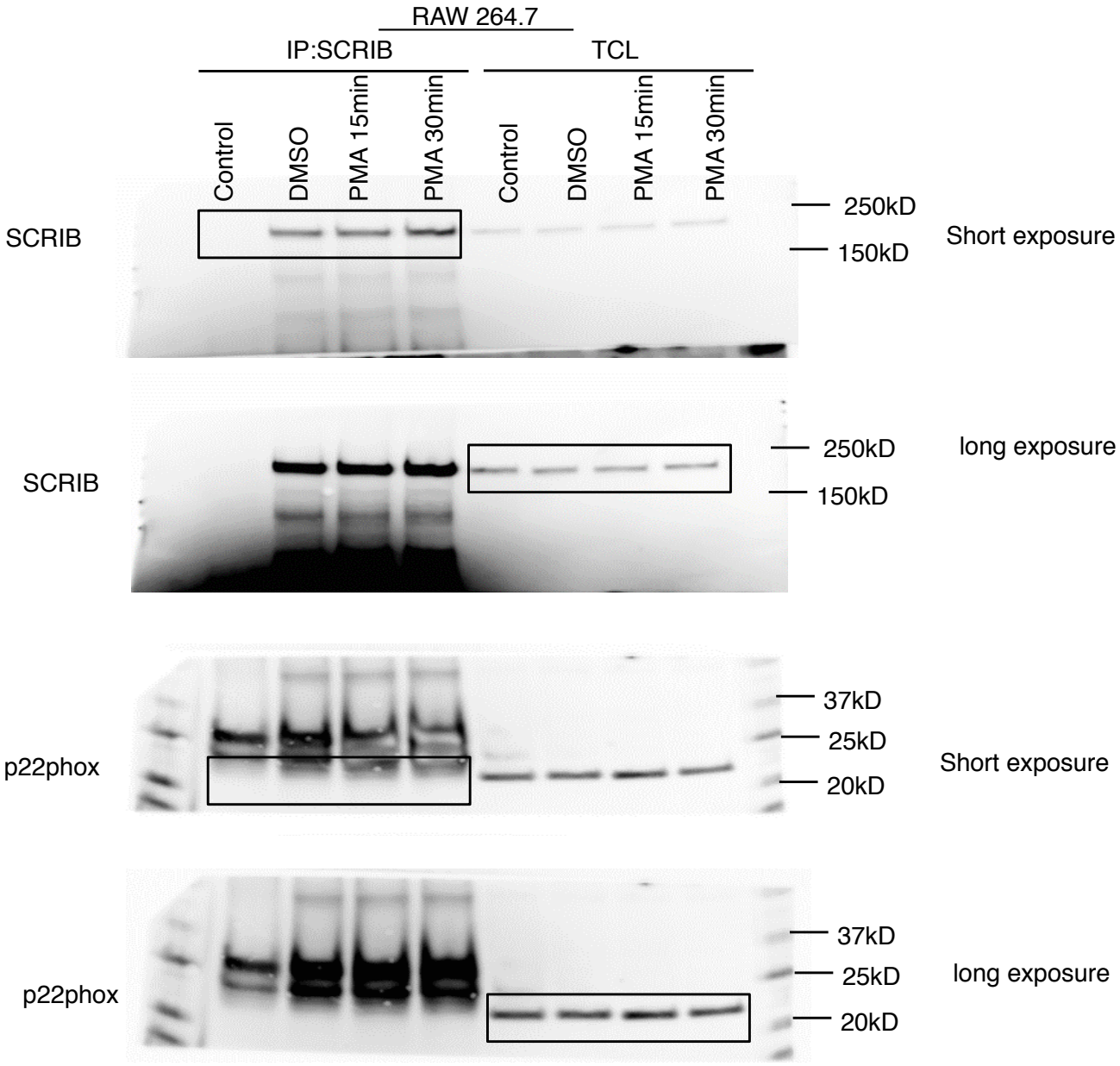

Supplementary Figure 6 continued

p

Fig.S4a

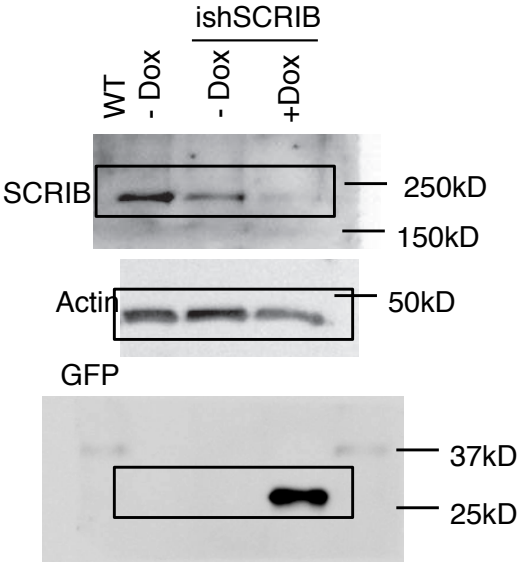

q

Fig.S5b

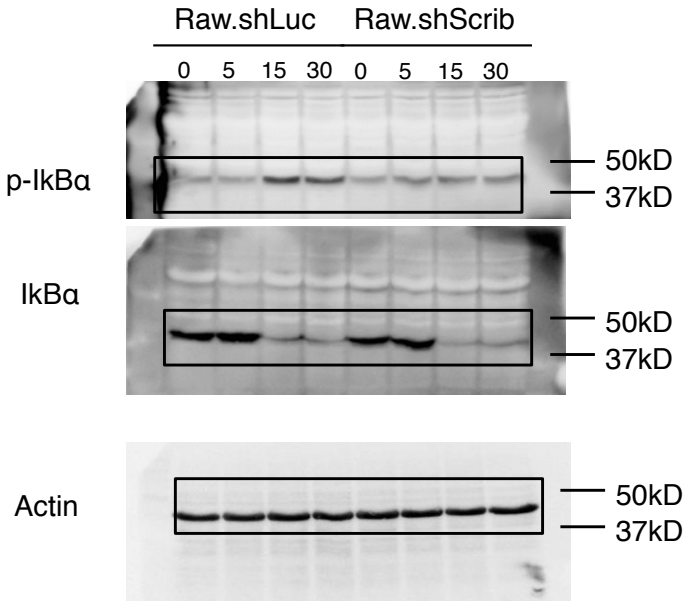

Supplementary Figure 6 continued

Supplementary Table Legends

Supplementary Table 1 List of antibodies used with supplier information and dilutions used.
Supplementary Table 2 List of primers and its sequence.
Supplementary Table 3 Statistics Source Data